

Bayesian Hierarchical Modelling of Initial-Final Mass Relations Across Star Clusters

Shijing Si,^{1★} David A. van Dyk,¹ Ted von Hippel,^{2,3} Elliot Robinson,⁴
Elizabeth Jeffery⁵, and David C. Stenning¹

¹*Statistics Section, Department of Mathematics, Imperial College London, London SW7 2AZ, UK*

²*Physical Sciences Department, Embry-Riddle Aeronautical University, Daytona Beach, FL, USA*

³*Institute of Astronomy, Madingley Road, Cambridge CB3 0HA, UK*

⁴*Argiope Technical Solutions, FL, USA*

⁵*Physics Department, California Polytechnic State University, San Luis Obispo, CA, USA*

Accepted XXX. Received YYY; in original form ZZZ

ABSTRACT

The initial-final mass relation (IFMR) of white dwarfs (WDs) plays an important role in stellar evolution. To derive precise estimates of IFMRs and explore how they may vary among star clusters, we propose a Bayesian hierarchical model that pools photometric data from multiple star clusters. After performing a simulation study to show the benefits of the Bayesian hierarchical model, we apply this model to five star clusters: the Hyades, M67, NGC 188, NGC 2168, and NGC 2477, leading to reasonable and consistent estimates of IFMRs for these clusters. We illustrate how a cluster-specific analysis of NGC 188 using its own photometric data can produce an unreasonable IFMR since its WDs have a narrow range of zero-age main sequence (ZAMS) masses. However, the Bayesian hierarchical model corrects the cluster-specific analysis by borrowing strength from other clusters, thus generating more reliable estimates of IFMR parameters. The data analysis presents the benefits of Bayesian hierarchical modelling over conventional cluster-specific methods, which motivates us to elaborate the powerful statistical techniques in this article.

Key words: methods: statistical – clusters: individual (Hyades, M67, NGC 188, NGC 2168 and NGC 2477)– techniques: photometric

1 INTRODUCTION

The initial-final mass relation (IFMR) provides a mapping between the zero-age main sequence (ZAMS) mass of a star

★ Contact e-mail: ss2913@ic.ac.uk

to its white dwarf (WD) mass and is vital to an understanding of mass loss during stellar evolution. Many researchers have investigated the IFMR using data from different star clusters, leading to numerous versions of the IFMR. For instance, [Williams et al. \(2004\)](#) presented an empirical IFMR based on spectroscopic analysis of seven massive WDs in NGC 2168 (M35). [Kalirai et al. \(2005\)](#) presented 24 new faint WDs in the open cluster NGC 2099 and determined an IFMR based on their high turnoff mass ($\sim 2.4M_{\odot}$). [Catalan et al. \(2008\)](#) explored the application of common proper motion pairs to improve the IFMR. [Salaris et al. \(2009\)](#) provided an empirical estimate of the IFMR using published results of WD properties in ten clusters. [Williams et al. \(2009\)](#) probed the empirical IFMR using WDs in the open cluster NGC 2168 (M35) at the high-mass end of the relation. [Cummings et al. \(2016\)](#) observed a sample of 10 WD candidates in the open cluster NGC 2323 and investigated a linear IFMR for high-mass ($\geq 0.9M_{\odot}$) WDs. By contrast, [Jeffery et al. \(2011\)](#) and [Zhao et al. \(2012\)](#) studied the IFMR in the low ZAMS mass range of $1-2M_{\odot}$. [Andrews et al. \(2015\)](#) identified 65 new wide double WDs and used them to constrain the IFMR.

[Stein et al. \(2013\)](#) treated the parametrised IFMR as cluster-specific parameters and developed simultaneous principled Bayesian estimates of all cluster-specific parameters, including those describing the IFMR. In addition, [Stein et al. \(2013\)](#) detected the disagreement of IFMRs from the Hyades, NGC 2168, and NGC 2477, which might be caused by many factors such as observation errors or metallicity differences among these clusters. In this paper, we approach the possible variation of IFMRs for different clusters with a Bayesian hierarchical model, which on average produces more accurate estimates of the IFMR(s).

Bayesian hierarchical modelling ([Gelman 2006](#); [Gelman et al. 2013](#)) is a statistical method that simultaneously fits object-specific parameters for multiple objects by pooling their data under one overall model. The resulting estimates from hierarchical models are shrinkage estimates ([Si et al.](#)

[2017a](#)) that generally have better statistical properties than do their unpooled counterparts. Bayesian hierarchical models have been used in numerous projects in astrophysics (e.g., [Jiao et al. 2016](#); [Shariff et al. 2016](#); [Mandel et al. 2017](#); [Si et al. 2017a,b](#); [Si & van Dyk 2018](#)). In the context of constraining the IFMR, [Andrews et al. \(2015\)](#) pooled 142 wide double WDs in a hierarchical model.

In this paper we propose a Bayesian hierarchical model for cluster IFMRs, show how this model can be fit using existing software, and use a suite of simulation studies to verify the statistical advantages of the resulting IFMR estimates. We aim to perform a comprehensive analysis of the IFMR by combining multiple star clusters into a hierarchical model. This allows us to simultaneously obtain better estimates of each cluster’s IFMR and to estimate the intrinsic variance of cluster-specific IFMRs. We apply the Bayesian hierarchical model using data from five clusters: the Hyades, M67, NGC 188, NGC 2168 and NGC 2477. We obtain the shrinkage estimates of IFMR parameters for these five clusters.

The paper is organised as follows. Section 2 summarises the cluster-specific Bayesian model for cluster parameters introduced by [Stein et al. \(2013\)](#) and proposes a hierarchical model to simultaneously fit multiple clusters. Section 3 presents a simulation study and demonstrates the advantages of the hierarchical model. In Section 4, we analyse five clusters via both the cluster-specific and hierarchical approaches, and illustrate the advantages of the latter approach. Section 5 covers the sensitivity analysis of the prior distribution used in the hierarchical model and membership of WDs in the cluster M67. The conclusion and discussion of the use of our statistical technique appears in Section 6.

2 STATISTICAL MODELS

In this Section, we review the Bayesian approach ([Stein et al. 2013](#)) to fit cluster-specific IFMR parameters and propose a hierarchical model that allows us to combine data from multiple clusters to simultaneously improve the estimate of the cluster-specific IFMR parameters and to explore the variability among IFMRs for different clusters.

2.1 Cluster-specific Analyses

Stein et al. (2013) develop a Bayesian approach for cluster parameters such as age, metallicity, and distance modulus while simultaneously estimating the IFMR for that cluster. They estimate the IFMR and other cluster parameters using a state-of-the-art Markov chain Monte Carlo (MCMC) algorithm and implement their methods using the software package BASE-9 (von Hippel et al. 2006; DeGennaro et al. 2009; van Dyk et al. 2009). BASE-9, short for Bayesian Analysis of Stellar Evolution with 9 parameters, deploys MCMC techniques to perform reliable Bayesian analysis for physical properties including age, distance modulus, metallicity and mass, based on the photometry of stars in a star cluster. Stein et al. (2013) fit one cluster at a time, i.e., cluster-specific analysis, so that each cluster has its own fitted IFMR.

In this paper we adopt a similar mathematical notation to that of Stein et al. (2013), while the subscript is extended to accommodate multiple star clusters. Suppose we have photometry for K star clusters, along with measurement errors. The number of stars in each cluster can vary, as can the number of photometric magnitudes observed for each cluster or even for the stars within the clusters. We use k to index clusters and i to index stars within clusters. Without loss of generality, we assume the number of stars within each cluster is N and that the observed photometry vector for star i within cluster k is \mathbf{X}_{ki} , with known measurement variance-covariance matrix $\mathbf{\Sigma}_{ki}$. We assume that age (θ_{age}), metallicity ($\theta_{[\text{Fe}/\text{H}]}$), distance modulus ($\theta_{\text{m-M}_V}$), and absorption (θ_{A_V}) are common to all stars in each cluster, and we denote them together as $\mathbf{\Theta}_k = (\theta_{\text{age},k}, \theta_{[\text{Fe}/\text{H}],k}, \theta_{\text{m-M}_V,k}, \theta_{\text{A}_V,k})$. We denote the parameters describing the IFMR of cluster k by α_k ; below we use a linear IFMR model so each α_k consists of an intercept and a slope. Since α_k is the same for all WDs in cluster k , we treat α_k as a cluster parameter. We denote the ZAMS mass of star i within cluster k as M_{ki} . Also, any star in the dataset may be a field star, i.e., not a member of a specific cluster. We define $\mathbf{Z}_k = (Z_{k1}, \dots, Z_{kN})$, where $Z_{ki} = 1$ if star i observed on the field of the sky with cluster k is indeed a cluster member, otherwise $Z_{ki} = 0$. (Of

Table 1. Cluster and stellar parameters.

Cluster parameters	
$\theta_{\text{age},k}$	\log_{10} age of the cluster k
$\theta_{[\text{Fe}/\text{H}],k}$	metallicity of the cluster k
$\theta_{\text{m-M}_V,k}$	distance modulus of the cluster k
$\theta_{\text{A}_V,k}$	absorption in V-band mag. of the cluster k
α_k	IFMR parameters of the cluster k
Stellar parameters	
M_{ki}	the initial mass of the observed star i of the cluster k
Z_{ki}	indicator for the membership of the observed star i in the cluster k

course Z_{ki} is unobserved and must be estimated.) See Table 1 for a summary of the model parameters.

We parametrise the IFMR of cluster k as a linear form

$$M_{\text{WD},ki} = \alpha_{k0} + \alpha_{k1}(M_{ki} - 3.0) \text{ for WD } i \text{ in cluster } k, \quad (1)$$

where $\alpha_k = (\alpha_{k0}, \alpha_{k1})$ are the intercept and slope parameters, and $M_{\text{WD},ki}$ is the mass of WD i within cluster k . Specifically α_{k0} is the WD mass of a star in cluster k with progenitor ZAMS mass equal to $3.0 M_{\odot}$. For every additional increment of $1.0 M_{\odot}$ in ZAMS mass, we expect the WD mass to increase by α_{k1} .

Though we have distinct evolution models for MS/RG and WD stars, we denote them indistinguishably by $\mathbf{G}(\cdot)$, which comprises MS/RG evolution models, WD cooling models, WD atmosphere models, and IFMR models. Because the expected photometric magnitudes of WDs depend on the WD masses, $\mathbf{G}(\cdot)$ must incorporate α_k . Thus, for the remainder of this article, the stellar evolution model $\mathbf{G}(\cdot)$, is viewed as a function of α_k in addition to $\mathbf{\Theta}_k$ and M_{ki} . Due to the computational complexity of stellar evolution models, in practice we employ a computer-based model to evaluate $\mathbf{G}(\cdot)$.

The cluster-specific model for cluster k is

$$\mathbf{X}_{ki} | (\mathbf{\Theta}_k, M_{ki}, \alpha_k) \sim \mathbf{N}(\mathbf{G}(\mathbf{\Theta}_k, M_{ki}, \alpha_k), \mathbf{\Sigma}_{ki}), \text{ if } Z_{ki} = 1, \quad (2)$$

where \mathbf{N} is a multivariate Gaussian distribution with mean $\mathbf{G}(\cdot)$ and variance-covariance matrix $\mathbf{\Sigma}_{ki}$, and $\mathbf{G}(\mathbf{\Theta}_k, M_{ki}, \alpha_k)$ is the predicted vector of photometric magnitudes for star i within cluster k . Eq. 2 summarises the probabilistic relationship between the photometry of stars that are members of cluster k (i.e., stars with $Z_{ki} = 1$) and the model param-

eters. If a star in dataset k is a field star (i.e., $Z_{ki} = 0$), we assume that its magnitudes are uniformly distributed on a hyper-rectangle which includes the full range of observed magnitudes of stars for that field. We use $p_{\text{field}}(\cdot)$ to denote the distribution of photometric magnitudes for field stars, which is simply the reciprocal of the volume of the hyper-rectangle. To be specific, for example, stellar cluster k has photometric magnitudes in the U, B, V filters. Then we find the range of U, B, V by using the maximum value of each filter minus its minimum and denote them ℓ_U, ℓ_B and ℓ_V . If a star with magnitudes \mathbf{X}_{ki} is a field star, its likelihood is $p_{\text{field}}(\mathbf{X}_{ki}) = \frac{1}{\ell_U \ell_B \ell_V}$. Though uniform model for field stars is unrealistic, [Stenning et al. \(2016\)](#) used a simulation study to demonstrate that the simple but physically unrealistic model can nevertheless identify field stars with a high level of accuracy. For details, refer to Page 10 of [Stenning et al. \(2016\)](#). Therefore, in this research I use uniform model for field stars in each cluster.

Taken together, this means that the likelihood function for cluster k is

$$L(\mathbf{M}_k, \boldsymbol{\Theta}_k, \mathbf{Z}_k, \boldsymbol{\alpha}_k | \mathbf{X}_k, \boldsymbol{\Sigma}_k) = \prod_{i=1}^N \left[\frac{Z_{ki}}{\sqrt{|2\pi\boldsymbol{\Sigma}_{ki}|}} \times \exp \left(-\frac{1}{2} \left(\mathbf{X}_{ki} - \mathbf{G}(\mathbf{M}_{ki}, \boldsymbol{\Theta}_k, \boldsymbol{\alpha}_k) \right)^\top \boldsymbol{\Sigma}_{ki}^{-1} \left(\mathbf{X}_{ki} - \mathbf{G}(\mathbf{M}_{ki}, \boldsymbol{\Theta}_k, \boldsymbol{\alpha}_k) \right) \right) + (1 - Z_i) p_{\text{field}}(\mathbf{X}_{ki}) \right], \quad (3)$$

where $\mathbf{M}_k = (M_{k1}, \dots, M_{kN})$, $\mathbf{X}_k = (X_{k1}, \dots, X_{kN})$, and $\boldsymbol{\Sigma}_k = (\boldsymbol{\Sigma}_{k1}, \dots, \boldsymbol{\Sigma}_{kN})$. The prior distribution for the parameters is assumed to be

$$p(\boldsymbol{\Theta}_k, \boldsymbol{\alpha}_k, \mathbf{M}_k, \mathbf{Z}_k) = p(\boldsymbol{\Theta}_k) p(\boldsymbol{\alpha}_k) p(\mathbf{M}_k) p(\mathbf{Z}_k) \quad (4)$$

$$= p(\theta_{\text{age},k}) p(\theta_{[\text{Fe}/\text{H}],k}) p(\theta_{m-M_V,k}) p(\theta_{\text{Av},k}) p(\boldsymbol{\alpha}_k) \times \prod_{i=1}^N p(M_{ki}) p(Z_{ki}).$$

Specifically, for $\theta_{\text{age},k}$, $\theta_{[\text{Fe}/\text{H}],k}$, $\theta_{m-M_V,k}$ and $\theta_{\text{Av},k}$ we use independent Gaussian prior distributions, with means set in accordance with recently published fits and variances chosen to be reasonably non-informative. In so doing, we eliminate the influence of prior distributions in our analyses. For the IFMR intercept α_{k0} we use a uniform prior distribution on the real line. For the IFMR slope α_{k1} we use a uniform distribution on the positive part of the real line, which excludes the possibility of a decreasing IFMR. The prior probability

of star i being a member of cluster k , $p(Z_{ki} = 1)$ is set based on the best available external information, typically using proper motions and/or radial velocities. Finally, we use one version of the initial mass function (IMF) of [Miller & Scalo \(1979\)](#) as the prior distribution of the ZAMS mass for star i , i.e.,

$$p(\log_{10}(M_i)) \propto \exp \left(-\frac{1}{2} \left(\frac{\log_{10}(M_i) + 1.02}{0.677} \right)^2 \right),$$

truncated to $0.1 M_\odot$ to $8 M_\odot$. The lower truncation is due to the fact that an initial mass of less than about $0.1 M_\odot$ is not sufficient to initiate the fusing of hydrogen into helium necessary to form a star. The upper truncation is because the star clusters we study are sufficiently old that any stars with an initial mass above $8 M_\odot$ would have used up their nuclear fuel long ago and become a neutron star or black hole, and thus would not be included in our observed data ([van Dyk et al. 2009](#)).

In their cluster-specific analysis of cluster k , [Stein et al. \(2013\)](#) based statistical inference, including parameters' estimates and error bars, on the joint posterior distribution,

$$p(\boldsymbol{\Theta}_k, \mathbf{M}_k, \mathbf{Z}_k, \boldsymbol{\alpha}_k | \mathbf{X}_k, \boldsymbol{\Sigma}_k) \propto p(\boldsymbol{\Theta}_k, \boldsymbol{\alpha}_k, \mathbf{M}_k, \mathbf{Z}_k) L(\mathbf{M}_k, \boldsymbol{\Theta}_k, \mathbf{Z}_k, \boldsymbol{\alpha}_k | \mathbf{X}_k, \boldsymbol{\Sigma}_k). \quad (5)$$

BASE-9 can draw a reliable sample for all parameters from their joint posterior distribution in Eq. 5. This is a cluster-specific study of the IFMRs because the fits of the IFMR parameters only rely on data from one cluster. We aim to perform a comprehensive analysis of the IFMR by combining multiple star clusters into a hierarchical model. This allows us to simultaneously obtain better estimates of each cluster's IFMR and to estimate the intrinsic variance of cluster-specific IFMRs.

2.2 Hierarchical Model

In this section, we describe how to pool data from multiple star clusters using a hierarchical model and how we fit this comprehensive model. For K star clusters, our hierarchical model is

$$\begin{cases} \mathbf{X}_{ki} | (\boldsymbol{\Theta}_k, \mathbf{M}_{ki}, \boldsymbol{\alpha}_k) \sim \mathcal{N}(\mathbf{G}(\boldsymbol{\Theta}_k, \mathbf{M}_{ki}, \boldsymbol{\alpha}_k), \boldsymbol{\Sigma}_{ki}), & \text{if } Z_{ki} = 1, \\ \text{where } \boldsymbol{\alpha}_k \sim \mathcal{N}(\boldsymbol{\gamma}, \boldsymbol{\Gamma}), & k = 1, \dots, K. \end{cases}$$

(6)

For field stars ($Z_{ki} = 0$), X_{ki} is uniformly distributed on the aforementioned hyper-rectangle. We set prior distributions on $\Theta_k, M_k, Z_k, k = 1, \dots, K$ as in the aforementioned cluster-specific analysis. We assume that IFMRs of different clusters follow a common bivariate normal distribution, which corresponds to the expectation that the IFMRs of different clusters, although not identical, are similar. The only new parameters in the hierarchical model in Eq. 6 are γ , the mean of the IFMR intercept and slope, and the Γ which is the variance-covariance matrix of IFMR parameters among the clusters. This assumption means that IFMR parameters of different clusters are from the same bivariate normal population with mean γ and variance-covariance matrix Γ . We must set prior distributions for γ and Γ and so we set $p(\gamma, \Gamma) = p(\gamma|\Gamma)p(\Gamma)$ with $p(\gamma | \Gamma)$ uniform on its range. For Γ , we set

$$\Gamma | \lambda_1, \lambda_2 \sim \text{Inverse-Wishart} \left(2\nu \begin{pmatrix} 1/\lambda_1 & 0 \\ 0 & 1/\lambda_2 \end{pmatrix}, \nu + 1 \right),$$

where the Inverse-Wishart¹ is the prior distribution for the variance matrix Γ given λ_1 and λ_2 , with $\lambda_1, \lambda_2 \sim \text{Inverse-Gamma}(1/2, 1/5000)$ ². It is sensible to take a diagonal scale matrix in the prior distribution of Γ because we parametrise the linear IFMR in eq. 1 in terms of $(M_{ki} - 3.0)$, where 3.0 is near the average of the ZAMS masses of the WDs in our clusters. This way of parametrisation decreases the correlation between IFMR intercept and slope, simplifying computation of the hierarchical model. Huang & Wand

¹ The Inverse-Wishart distribution is the conjugate prior distribution for the variance-covariance matrix of a multivariate normal distribution. The Inverse-Wishart distribution is parametrised in terms of its scale matrix Ψ and its degrees of freedom ν ; its probability density function is

$$p(X|\Psi, \nu) = \frac{|\Psi|^{\frac{\nu}{2}}}{2^{\frac{\nu p}{2}} \Gamma_p(\frac{\nu}{2})} |X|^{-\frac{\nu+p+1}{2}} e^{-\frac{1}{2}tr(\Psi X^{-1})},$$

where Γ_p is the multivariate gamma function and tr is the trace function.

² The Inverse-Gamma is the reciprocal of of Gamma distribution, parametrised by its shape α and its rate β ; its density function is

$$p(x|\alpha, \beta) = \frac{\beta^\alpha}{\Gamma(\alpha)} x^{-\alpha-1} \exp\left(-\frac{\beta}{x}\right),$$

where Γ is the Gamma function.

(2013) suggests setting $\nu = 2$ for a weakly informative prior distribution on Γ . In this paper, we set $\nu = 2$ and take a weakly informative distribution for Γ , which reduces the effect of the prior distribution and produces estimates that mostly depend on the photometric data.

We fit the hierarchical model Eq. 6 in a Bayesian manner, and it infers all parameters via their marginal posterior distributions by integrating out other parameters from their joint posterior distribution. MCMC techniques are employed to simulate samples of all parameters. For details about the statistical inference of hierarchical models, see Gelman et al. (2013); Si et al. (2017a). The joint posterior density for all parameters in Eq. 6 is

$$\begin{aligned} & p(\gamma, \Gamma, \lambda_1, \lambda_2, \Theta_1, M_1, Z_1, \alpha_1, \dots, \Theta_K, M_K, Z_K, \alpha_K \\ & | X_1, \Sigma_1, \dots, X_K, \Sigma_K) \\ & = p(\lambda_1)p(\lambda_2)p(\gamma, \Gamma | \lambda_1, \lambda_2) \times \prod_{k=1}^K \\ & \left(p(\Theta_k)p(M_k, Z_k)p(\alpha_k | \gamma, \Gamma)L(M_k, \Theta_k, Z_k, \alpha_k | X_k, \Sigma_k) \right) \end{aligned} \quad (7)$$

In Appendix A we present a two-stage algorithm that draws a reliable sample for parameters in the joint posterior in Eq. 7. In the first stage, it draws a sufficient sample of parameters from the cluster-specific analysis in Eq. 5 to be used as the proposal distribution in a Metropolis-Hastings sampler with target distribution equal to the hierarchical posterior distribution in Eq. 7. This strategy tackles the high-dimensional sampling problem in Eq. 7 by taking advantage of the cluster-specific analyses.

3 SIMULATION STUDY

To illustrate the statistical advantages of our hierarchical model, we simulate $K = 10$ star clusters with BASE-9 and we recover their IFMRs via both cluster-specific and hierarchical analyses. We simulate the cluster parameters using the distributions in Table 2. These parameter values in Table 2 are set to be similar to those of the observed star clusters that we analyse in Section 4. To mimic the errors of the observed photometry, we compute the average standard deviations for filters B, V , and I of the WDs in the datasets analysed in Section 4 and use them as the corresponding

Table 2. Parameter distributions for Simulated Clusters

$\theta_{\text{age},k} \sim N(9.0, 0.1^2),$
$\theta_{[\text{Fe}/\text{H}],k} \sim N(-0.08, 0.05^2),$
$\theta_{\text{m-MV},k} = 10.0,$
$\theta_{\text{Av},k} \sim N(0.51, 0.43^2)$ truncated to positive values,
$\alpha_k \sim N_2(\gamma_0, \Gamma_0)$, with
$\gamma_0 = \begin{pmatrix} 0.722 \\ 0.107 \end{pmatrix}, \Gamma_0 = \begin{pmatrix} 0.05^2 & -0.2 \cdot 0.05 \cdot 0.02 \\ -0.2 \cdot 0.05 \cdot 0.02 & 0.02^2 \end{pmatrix}$

errors in the simulated datasets. Specifically, the observed errors for B, V, I are $\sigma_B = 0.026, \sigma_V = 0.035$, and $\sigma_I = 0.185$.

After simulating the parameters $\theta_{\text{age},k}, \theta_{[\text{Fe}/\text{H}],k}, \theta_{\text{m-MV},k}$, and $\theta_{\text{Av},k}$ of cluster k , we simulate photometric data for each star in the cluster using BASE-9 (see the BASE-9 User’s Manual, von Hippel et al. 2014). For each cluster, we simulate 200 MS/RG stars brighter than $V = 15$ and 10 WDs. Subsequently, we recover the parameters of each cluster by fitting the simulated datasets with BASE-9 using the cluster-specific analysis described in Section 2.1. In so doing, we obtain a sample of the parameters for each cluster from its posterior distribution, see Eq. 5. For this paper, we employ the Dotter et al. (2008, as updated at <http://stellar.dartmouth.edu/~models/>) MS/RG models, Montgomery et al. (1999) WD interior models, Bergeron et al. (1995, with updates posted online) WD atmospheres, and the IFMR model in Eq. 1.

We repeat the data generation and parameter estimation 25 times, record results from both the hierarchical and case-by-case methods. We compare estimates in terms of two criteria: i.) root mean squared error (RMSE) of point estimates, and 2.) actual versus nominal coverage probabilities of interval estimates. When we require point estimates, we utilise posterior means from MCMC samples, and for interval estimates we use the 68.3% credible intervals from posterior distributions by finding the 15.8% and 84.1% quantiles from the MCMC samples.

Table 3 presents the RMSE of point estimates and the actual coverage probabilities of 68.3% credible interval estimates for IFMR constants and slopes using two methods: Bayesian hierarchical modelling and case-by-case. The 68.3% confidence intervals of the coverage probabilities are computed with the Clopper-Pearson exact method (Clopper & Pearson 1934). From this table, the RMSE of hierarchical

estimates of IFMR constants is 0.067, about a third of that from the case-by-case method (0.202). The performance of hierarchical modelling is even better on IFMR slope with its RMSE, 0.019, about 1/17 of that from the case-by-case analysis. In terms of interval estimates of IFMR parameters, the case-by-case (cluster-specific) method has actual coverage probabilities, 80% and 84.4% for IFMR constant and slope respectively, higher than the nominal value, 68.3%. The actual coverage probabilities of interval estimates from Bayesian hierarchical modelling, 76.4% and 62.8% for IFMR constant and slope respectively, are closer to the nominal value. In summary, the estimates of IFMR parameters from the hierarchical fits outperform that from case-by-case fits in terms of RMSE and coverage property.

Here are population-level parameters: the population mean of IFMR parameters, $\gamma = (\gamma_1, \gamma_2)$, in which γ_1 and γ_2 are the mean of IFMR constants and slopes, respectively; the population variance-covariance matrix of IFMR parameters,

$$\Gamma = \begin{pmatrix} \sigma_1^2 & \rho\sigma_1\sigma_2 \\ \rho\sigma_1\sigma_2 & \sigma_2^2 \end{pmatrix},$$

in which σ_1, σ_2 and ρ are the standard deviations of IFMR constants, slopes and the correlation between them, respectively. In our analysis, IFMR is parameterised as $M_{\text{final}} = \alpha_0 + \alpha_1(M_{\text{initial}} - 3.0)$, but many researchers use another form $M_{\text{final}} = \tilde{\alpha}_0 + \alpha_1 M_{\text{initial}}$, $\tilde{\alpha}_0 = \alpha_0 - 3\alpha_1$, which is the intercept of the IFMR line with the $M_{\text{initial}} = 0.0$. To make our results comparable with others, we transform our results in the $\tilde{\alpha}_0$ (intercept) and α_1 form. We denote the population mean of intercept at 0 to be $\tilde{\gamma}_1$.

Table 4 presents the RMSE of point estimates and the actual coverage probabilities of 68.3% credible interval estimates for population-level parameters using the Bayesian hierarchical approach. The 68.3% confidence intervals of the coverage probabilities are computed with the Clopper-Pearson exact method (Clopper & Pearson 1934). The case-by-case method does not pool star clusters into a population, so it fails to produce estimates of the population. From this table, the RMSE of Bayesian hierarchical estimates of population-level parameters are small except σ_1 and ρ . From the actual coverage property of interval estimates, the hierarchical method tends to produce over-covered interval es-

Table 3. RMSE and coverage probabilities (CP) of 68.3% credible intervals (CI) for IFMR parameters from Bayesian hierarchical modelling and case-by-case analyses.

Items	Hierarchical			Case-by-case		
	RMSE	CP	68.3% CI	RMSE	CP	68.3% CI
IFMR Const.	0.067	0.764	(0.734, 0.792)	0.202	0.8	(0.771, 0.826)
IFMR Slope	0.019	0.628	(0.595, 0.660)	0.331	0.844	(0.818, 0.867)

Table 4. RMSE and coverage probabilities (CP) of 68.3% credible intervals (CI) for population-level parameters from the Bayesian hierarchical modelling.

Items	Hierarchical		
	RMSE	CP	68.3% CI
γ_1	0.021	0.92	(0.824, 0.972)
γ_2	0.009	0.68	(0.561, 0.782)
$\tilde{\gamma}_1 = \gamma_1 - 3\gamma_2$	0.034	0.76	(0.644, 0.851)
σ_1	0.057	0.6	(0.48, 0.711)
σ_2	0.007	0.88	(0.777, 0.945)
ρ	0.281	0.96	(0.874, 0.993)

estimates. For parameters like γ_2 , $\tilde{\gamma}_1$ and σ_1 , their interval estimates perform well, and their actual coverage probabilities are close to the nominal level 68.3%, and their 68.3% confidence interval of coverage contains the nominal value. The difficulty of Bayesian hierarchical method in estimating population-level parameters is mainly due to two reasons, the small number of objects, $I = 10$. Other research have also reported and discussed this problem, refer to [Browne & Goldstein \(2002\)](#); [Browne et al. \(2006\)](#) for more details.

To further investigate the advantage of the hierarchical analysis in Eq. (6), we take one group of 10 simulated clusters as an example and compare the estimates of IFMR parameters from the case-by-case and Bayesian hierarchical fits. After we obtain the MCMC sample for the IFMR parameters, we use its sample means as point estimates of α_k , $k = 1, \dots, K$. We denote the sample means of IFMR parameters from the cluster-specific fits as $\hat{\alpha}_k^{\text{CS}}$, and denote those from the hierarchical analysis as $\hat{\alpha}_k^{\text{Hier}}$.

We simultaneously analyse the 10 simulated datasets using a hierarchical model, obtaining a sample of all parameters from the posterior distribution given in Eq. 7. In this paper, we focus on estimating the IFMR parameters $\alpha_1, \dots, \alpha_K$. After we obtain the MCMC sample for the IFMR parameters, we use its sample means as point estimates of α_k , $k = 1, \dots, K$. We denote the sample means of IFMR pa-

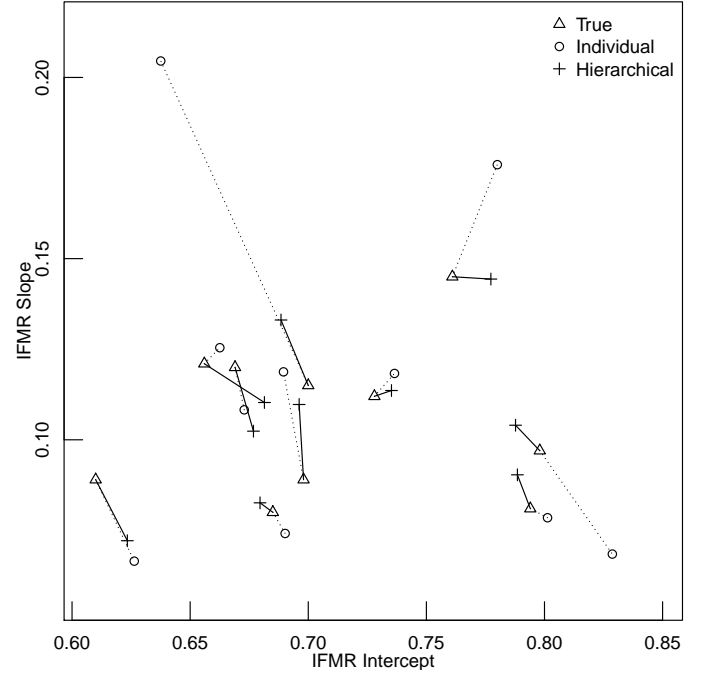


Figure 1. Scatter plot of IFMR intercept vs slope. Triangles, circles, and plus signs represent true values, cluster-specific and hierarchical estimates of IFMR parameters for 10 simulated clusters. Dotted and solid lines connect the cluster-specific and hierarchical estimates to their true values for one particular cluster.

rameters from the cluster-specific analyses as $\hat{\alpha}_k^{\text{CS}}$, and denote those from the hierarchical analysis as $\hat{\alpha}_k^{\text{Hier}}$.

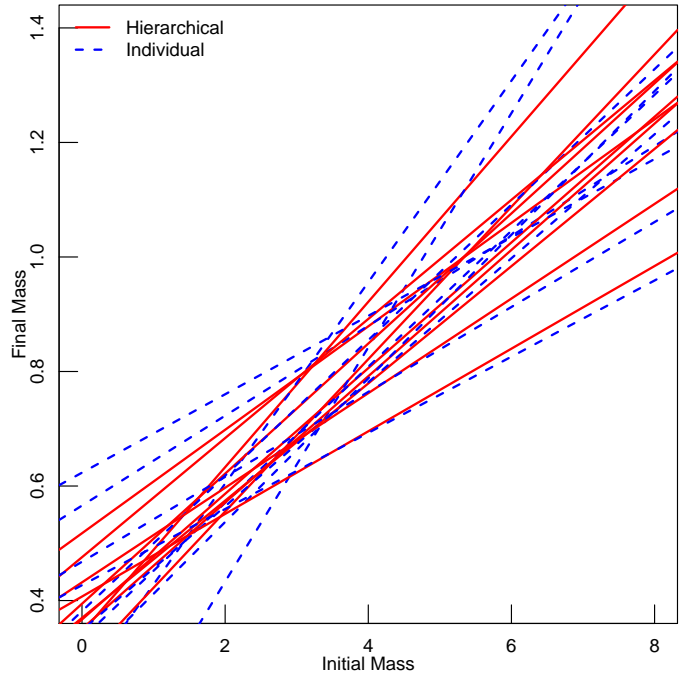
Fig. 1 presents the scatter plot of IFMR intercept versus slope, with points of three different shapes (triangle, circle, plus sign) representing true values, cluster-specific (individual) and hierarchical estimates for IFMR parameters for those 10 simulated clusters. To compare the distances between estimates and true values, for one particular cluster, we connect its true values to cluster-specific and hierarchical estimates with dotted and solid lines, respectively. From Fig. 1, it can be observed that for most clusters the hierarchical model yield more precise estimates of IFMR parameters than the cluster-specific method.

Table 5. Point estimates of the IFMR parameters for the 10 simulated clusters from both the cluster-specific and hierarchical analyses. Standard errors of estimates are presented in parentheses.

Cluster (k)	True Values		Cluster-specific Estimates		Hierarchical Estimates	
	IFMR Const. ($\hat{\alpha}_{k0}$)	IFMR Slope ($\hat{\alpha}_{k1}$)	IFMR Const. ($\hat{\alpha}_{k0}^{CS}$)	IFMR Slope ($\hat{\alpha}_{k1}^{CS}$)	IFMR Const. ($\hat{\alpha}_{k0}^{Hier}$)	IFMR Slope ($\hat{\alpha}_{k1}^{Hier}$)
1	0.794	0.081	0.801 (0.018)	0.078 (0.018)	0.789 (0.024)	0.090 (0.020)
2	0.761	0.145	0.780 (0.039)	0.176 (0.042)	0.777 (0.032)	0.144 (0.020)
3	0.700	0.115	0.638 (0.048)	0.205 (0.061)	0.688 (0.036)	0.133 (0.023)
4	0.698	0.089	0.690 (0.030)	0.119 (0.029)	0.696 (0.026)	0.110 (0.021)
5	0.656	0.121	0.663 (0.040)	0.125 (0.036)	0.681 (0.030)	0.110 (0.023)
6	0.728	0.112	0.736 (0.020)	0.118 (0.022)	0.735 (0.019)	0.114 (0.016)
7	0.798	0.097	0.829 (0.047)	0.068 (0.046)	0.788 (0.030)	0.104 (0.032)
8	0.669	0.120	0.673 (0.020)	0.108 (0.032)	0.677 (0.017)	0.102 (0.022)
9	0.685	0.080	0.690 (0.049)	0.074 (0.028)	0.680 (0.037)	0.083 (0.022)
10	0.610	0.089	0.626 (0.036)	0.067 (0.027)	0.623 (0.031)	0.072 (0.025)

Table 5 reports the true values of the 10 simulated IFMR parameters and their estimates from both the hierarchical and cluster-specific analyses. For most of the clusters, the hierarchical estimates are closer to their true values than are their cluster-specific counterparts. Specifically, the hierarchical estimates are better for clusters 2, 3, 4, 6, 7, 9, and 10. From the aspect of standard errors of estimates in parentheses, the hierarchical modelling outperforms cluster-specific fits, since it produces smaller standard errors for every cluster except cluster 1. Overall, the RMSE of the hierarchical estimates is 0.012, i.e., the average deviation of hierarchical estimates from the true values is 0.012, while that of the cluster-specific estimates is 0.029, more than twice the hierarchical value.

Fig. 2 illustrates the recovered IFMRs for the 10 simulated clusters. The red solid lines are the hierarchical fits and the blue dashed lines are the cluster-specific fits. A key feature of the hierarchical estimates is that they tend to cluster toward the centre, displaying the shrinkage effect (Morris & Lysy 2012; Gelman et al. 2013) of hierarchical models. Statistically, this property stems from the assumption that the IFMR parameters of different clusters are generated from the same bivariate normal distribution in Eq. 6. Astrophysically, this corresponds to the expectation that the IFMRs of different clusters, although not identical, are similar. Our Bayesian hierarchical model is similar in spirit to the method in Si et al. (2017a), where we pool ten Galactic halo white dwarfs in a Bayesian hierarchical analysis in which we assume that their ages follow a common normal distribution. Si

**Figure 2.** Estimated IFMR parameters for 10 simulated clusters using both the hierarchical (red solid lines) and cluster-specific (blue dashed lines) analyses.**Table 6.** CPU Times of two methods in the IFMR project

Algorithms	Time
Case-by-case Analysis	About 30 hours for 10000 draws
Hierarchical Model Two-stage	About 30 hours and 10 minutes for 10000 draws

et al. (2017b) verifies that even when this normality assumption is violated, estimates based on the Bayesian hierarchical model still outperform their case-by-case counterparts.

Table 6 presents the computing time of the case-by-case

and Bayesian hierarchical fits. Because each star cluster may have different number of stars, which affects the computing time, here is the time for a cluster consisting of 200 stars, each of which has three photometric magnitudes U , V , and I . The case-by-case analysis takes about 30 hours for 10000 draws and the hierarchical modelling with two-stage sampler uses the case-by-case fits and costs additional 10 minutes to produce estimates from the hierarchical model. Throughout this research, all timings are carried out on a Ubuntu linux server that has 64 AMD Opteron 2.5 GHz processors. We wrote code in R programming language (R Core Team 2017) to undertake computations. On other computer systems or programming languages, the relative CPU times of different methods should be similar.

In summary, the Bayesian hierarchical approach with a two-stage sampler produces shrinkage estimates of the IFMR parameters that have smaller RMSEs than the case-by-case analysis. Also, if the case-by-case samples are available, it only takes the two-stage algorithm ten minutes to obtain the estimates under the hierarchical model. So we recommend readers to use our two-stage algorithm to fit hierarchical models.

4 DATA ANALYSIS

In this section we deploy both the cluster-specific and hierarchical analyses using photometry for five star clusters: the Hyades, M67, NGC 188, NGC 2168, and NGC 2477. In the data analysis, we use Montgomery et al. (1999) WD interior models and Bergeron et al. (1995) WD atmospheres models. For the MS/RG models, we use Dotter et al. (2008) models for all clusters except NGC2168, which is too young for the Dotter et al. (2008) models, so we choose Girardi et al. (2000) models instead.

When BASE-9 fits a star cluster, it uses the MS/RG model to estimate the age and other parameters of the cluster based on main sequence, main sequence turn-off, subgiant branch and red giant stars, and uses the WD models to estimate the ages of the cluster WDs, then it computes the precursor ages for the WDs and uses the MS/RG models again to determine the initial (ZAMS) masses of

the WDs. For the Dotter et al. models, the highest mass precursors are $\sim 3.5M_{\odot}$ for the metallicity of NGC 2477, and BASE-9 therefore extrapolated the $\log_{10}(\text{age})$ versus precursor mass relation. This is not an ideal approach. Nevertheless, comparing the Dotter et al. (2008) model extrapolation to the Girardi et al. (2000) models yielded similar results with the Dotter et al. precursor masses being consistently lower by just 13.4% to 17.5% than the Girardi et al. precursor masses. We return to this point in Section 4.2 when we examine and compare the cluster IFMRs.

4.1 Cluster-specific Analysis

We perform the cluster-specific analysis developed by Stein et al. (2013), which uses BASE-9 to deliver MCMC samples of all model parameters from the respective posterior distribution for each cluster. The prior distributions that we use for distance moduli, metallicities, and absorptions of the five clusters are shown in Table 7. Because the MS/RG models tend to poorly predict the photometry of faint main sequence stars, we removed main sequence stars with V magnitudes greater than the cluster-specific thresholds given in Table 7. Table 7 also gives the references where we obtain the cluster-specific prior distributions and cut-off for the V magnitude. For reading continuity, we present the photometric data and errors for WDs in these five clusters in Tables B1–B3 in Appendix B.

For NGC 2477 we set the prior standard deviations for the distance modulus, absorption, and metallicity to zero. The reason for doing this is that NGC 2477 suffers differential reddening, which is not within the BASE-9 model. Stein et al. found that by fixing these three cluster parameters at certain reasonable values consistent with literature estimates, BASE-9 produces good results for the age and IFMR parameters of NGC 2477. In our analysis, we follow the method of Stein et al. (2013).

Here we elaborate on the prior distribution of distance modulus for the Hyades in Table 7. In the case-by-case (cluster-specific) analysis via BASE-9, we assume that all

Table 7. Prior distributions, maximum V magnitudes, and references for the five analysed clusters

Cluster	Dist. Mod.	Metallicity	Absorption ^a	Max. V	Reference
Hyades	$N(0.0, 0.03^2)^b$	$N(0.07, 0.05^2)$	$N(0.009, 0.006^2)$	4.5	DeGennaro et al. (2009); Stein et al. (2013)
M67	$N(9.62, 0.091^2)$	$N(-0.009, 0.009^2)$	$N(0.127, 0.013^2)$	15.0	VandenBerg & Stetson (2004); Taylor (2006)
NGC 188	$N(11.24, 0.1^2)$	$N(-0.03, 0.1^2)$	$N(0.27, 0.1^2)$	15.5	von Hippel & Sarajedini (1998) and Meibom et al. (2009)
NGC 2168	$N(10.3, 0.1^2)$	$N(-0.2, 0.3^2)$	$N(0.682, 0.1^2)$	30.0	Stein et al. (2013)
NGC 2477	$N(11.46, 0.0^2)$	$N(-0.1, 0.0^2)$	$N(0.75, 0.0^2)$	15.5	Jeffery et al. (2011); Stein et al. (2013)

^a All prior distributions of Absorptions are truncated to positive values.

^b The Hyades is analysed with apparent magnitudes converted to absolute magnitudes.

stars in a specific cluster have the same distance modulus. This assumption is approximately true for clusters fairly far from the Earth. For the Hyades, due to the fact that its proximity (~ 50 pc) to the Solar System is comparable to its depth ($\sim 10 - 20$ pc), its member stars have significantly different distances, which violates the equal distance assumption in the BASE-9. **To address this problem, DeGennaro (2009) adjusted the magnitudes of each star for its distance using the precise distance estimates obtained by de Bruijne, J. H. J. et al. (2001).** Each Hyades star was offset to a nominal distance modulus of $m - M_V = 0.0$, i.e., 10 pc. We therefore set the prior distance modulus to be a Gaussian distribution with mean 0. Additionally, because the Hyades is well-studied and the uncertainty of its distance modulus is small, we take 0.03 as the prior standard deviation. After we obtain the MCMC samples for the Hyades from the case-by-case analysis, we add the average distance modulus from multiple studies, 3.40, (Perryman et al. 1998; DeGennaro 2009) to the MCMC sample of distance modulus and thereby recover the posterior sample of distance modulus for Hyades with BASE-9. For details, refer to DeGennaro (2009); DeGennaro et al. (2009); Stein et al. (2013).

The MCMC samples from the cluster-specific analyses appear in Fig. 3. Each row corresponds to one cluster, and the columns provide scatter plots of various parameter combinations. Because the prior standard deviations of metallicity, distance modulus, and absorption are set to zero for NGC 2477, the scatter plots of age–metallicity, age–distance, age–absorption degenerate into lines. The scatter plot of the IFMR parameters for NGC 2477 has two separate modes. The upper mode, accounting for 90.44% of the distribution,

tends to have a larger IFMR slope than the lower one, constituting 9.56% of the posterior distribution. The most likely explanation for the bimodal nature is uncertainty in cluster membership of one or more stars.

The rightmost column of Fig. 3 displays the scatter plots of the IFMR parameters for the five clusters under the cluster-specific analyses. For all of the clusters except NGC 188, the range of the IFMR intercept is 0.55 to 0.95 and that of the IFMR slope is 0.0 to 0.4, which are both quite consistent with the results in Salaris et al. (2009) and Williams et al. (2009). However, the IFMR parameters for NGC 188 are both far from their commonly accepted ranges. This appears to be because all of the WDs in NGC 188 have similar ZAMS masses (1.17 to 1.24 M_\odot), but their WD masses vary significantly (0.52 to 0.80 M_\odot). We do not address these particular properties of NGC 188 WDs, instead leaving them to be discussed in Section 4.2. This difference in the fitted IFMRs provides an opportunity to test the power of the hierarchical model. In the next section, we simultaneously analyse the five clusters with a hierarchical model. This allows us to borrow strength among the clusters and provides more reliable estimates of the IFMR parameters, particularly for NGC 188.

The estimates of cluster parameters from the cluster-specific analyses are shown in the lower part in Table 8. The IFMR parameters – intercept and slope – are in the last two columns. From the cluster-specific analyses, the estimates of the IFMR parameters vary significantly from cluster to cluster. Most noticeably, the IFMR estimates of NGC 188 are unrealistic with very large standard errors. The other star clusters also exhibit significant differences in

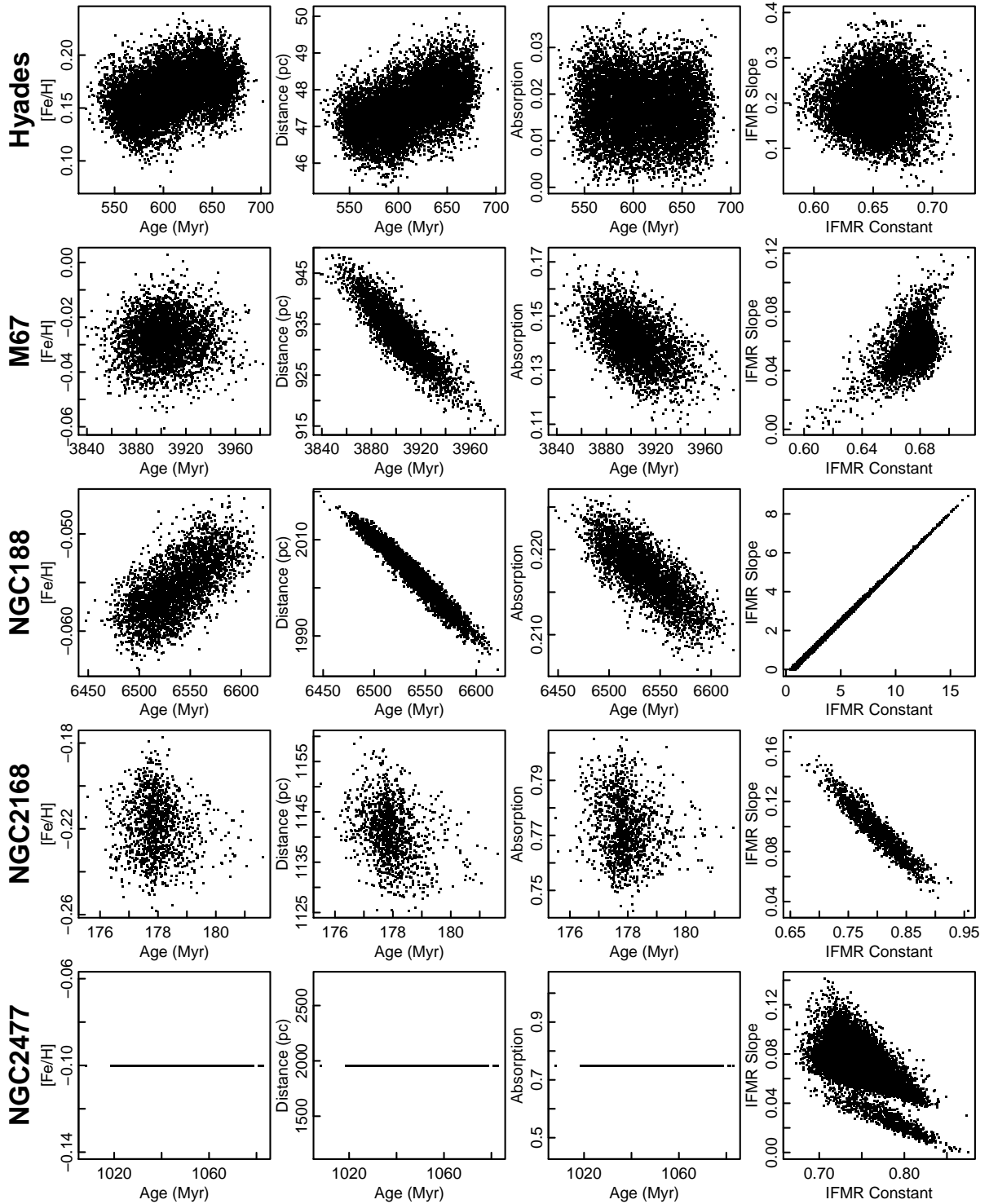


Figure 3. Cluster-specific results: projections of the joint posterior distributions onto the two dimensional planes of (from left to right) age–metallicity, age–distance, age–absorption, and IFMR intercept–IFMR slope for the five analysed clusters.

their estimated IFMR parameters, especially in the IFMR slopes. We do not know the exact reasons for these divergences. One possible explanation is that we assume each star cluster has its own linear IFMR,

which affects the estimates of the IFMR parameters. Yet many researchers argue that the IFMR is non-linear (Marigo, P. & Girardi, L. 2007; Meng et al. 2008; Choi et al. 2016). Alternatively cluster metal-

licity may affect the IFMR (Meng et al. 2008; Zhao et al. 2012). The metallicities of these five clusters vary significantly, which might cause the divergences of their IFMR parameters.

Here we investigate the sensitivity of the cluster's IFMR parameters to its WD mass range. We still assume the linear functional form of the IFMRs and use NGC 2477 as an example. NGC 2477 has seven WDs in the original cluster-specific analysis and among them three have ZAMS between 2 to 4 M_{\odot} , with the other four above 4 M_{\odot} . In this test we remove the three low mass WDs below 4 M_{\odot} from NGC 2477, use BASE-9 to fit the modified dataset and compare the fitted IFMR parameters. Fig. 4 displays the histograms of IFMR parameters for NGC 2477 under the two conditions: including all seven WDs and only including the four WDs above 4 M_{\odot} . The left and right panels show the posterior distributions of IFMR constant and slope for NGC 2477, respectively. The solid and dotted histograms represent results from the cases: 1) all seven WDs in NGC 2477 are used and 2) only the WDs above 4 M_{\odot} are used, respectively. The histograms of both IFMR constant and slope remain essentially the same in both cases (with tiny difference caused by simulation errors), which means that the estimates of IFMR parameters for NGC 2477 vary insignificantly even as its initial mass range diminishes. This small experiment implies that at least for the current NGC 2477 data, that the progenitor mass range does not affect the IFMR parameters.

Studies have shown that the metallicity may affect the IFMR parameters of a cluster (e.g., Kalirai et al. 2005; Catalan et al. 2008; Meng et al. 2008; Zhao et al. 2012). We have explored the quantity and quality of data required to test whether the IFMR intercept and slope depends on metallicity. We can investigate the effect of metallicity on the IFMR parameters via an extension of our Bayesian hierarchical model. To achieve this, we adjust the bivariate Gaussian assumption on IFMR parameters

α_k in Eq. 6 to be

$$\alpha_k = \begin{pmatrix} \alpha_{k0} \\ \alpha_{k1} \end{pmatrix} \sim N(\mathbf{B}\eta_k, \mathbf{\Gamma}),$$

with

$$\mathbf{B} = \begin{pmatrix} b_{11} & b_{12} \\ b_{21} & b_{22} \end{pmatrix}, \eta_k = \begin{pmatrix} 1 \\ \theta_{[\text{Fe}/\text{H}],k} \end{pmatrix},$$

where matrix \mathbf{B} is the effect of metallicity $\theta_{[\text{Fe}/\text{H}],k}$ of cluster k on its IFMR parameters α_k . Our two-stage algorithm has the capacity to fit this complicated hierarchical model. This model introduces four more parameters in the effect matrix \mathbf{B} , yet at present we only have five clusters in this study. So for the present study we maintain the simple model of Eq. (6) and we plan to investigate the effect of metallicity on the IFMR once we have a sufficient number of stellar clusters.

4.2 Hierarchical Analysis

In this section, we present the result obtained under the hierarchical analysis in Section 2.2. We deploy the two-stage algorithm in Appendix A to obtain the MCMC samples for all model parameters. For simplicity, we compute posterior sample means and standard deviations to summarise the posterior distributions of each parameter. Table 8 compares the estimates and error bars for all five clusters obtained using the hierarchical and cluster-specific methods. In all five cases, the estimates of $\log_{10}(\text{Age})$, $m - M_V$, $[\text{Fe}/\text{H}]$ and absorption are nearly the same for the hierarchical and cluster-specific fits. The estimates of the IFMR parameters for NGC 188, however, differ substantially. From the cluster-specific analysis, the posterior mean of the IFMR for NGC 188 is $M_{\text{WD}} = 4.522 + 2.195(M_{\text{ZAMS}} - 3.0)$. This implies that a star with ZAMS mass 3 M_{\odot} has a WD mass of 4.522 M_{\odot} and that WD mass increases by 2.195 M_{\odot} for each additional M_{\odot} in its ZAMS mass. Clearly, this result is nonsense: it violates conservation of mass. The reason the cluster-specific analysis results in this bizarre IFMR is that the ZAMS masses of WDs in NGC 188 are in a narrow range, 1.17 to 1.33 M_{\odot} , so they fail to constrain the IFMR parameters over the whole ZAMS mass range. By contrast, the hierar-

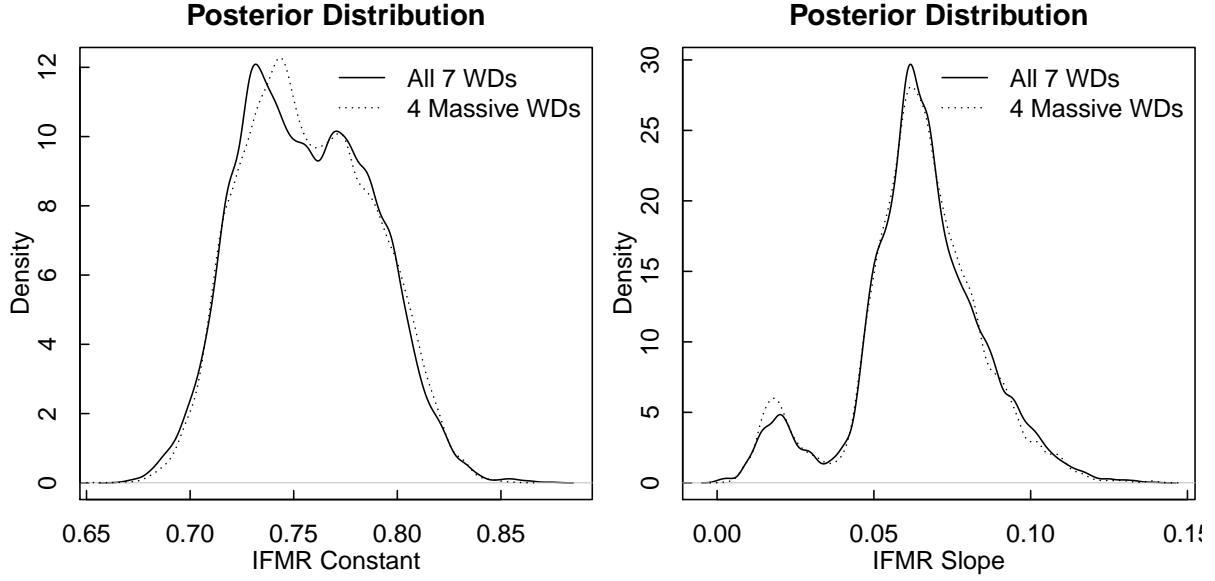


Figure 4. Two fits of NGC 2477: solid line is from the original fit (including all WDs in NGC 2477) and dotted line is from the fit after three less massive white dwarfs are removed.

Table 8. Parameter estimates for the five clusters under both the hierarchical and cluster-specific fits

	Cluster	$\log_{10}(\text{Age})$	$m - M_V$	[Fe/H]	Absorption	IFMR Intercept	IFMR Slope
Hierarchical Estimates	Hyades	8.773 ± 0.026	-0.000 ± 0.030	0.157 ± 0.020	0.017 ± 0.006	0.660 ± 0.020	0.140 ± 0.050
	M67	9.591 ± 0.002	9.850 ± 0.010	-0.029 ± 0.007	0.142 ± 0.008	0.680 ± 0.010	0.060 ± 0.010
	NGC188	9.815 ± 0.002	11.510 ± 0.010	-0.056 ± 0.003	0.218 ± 0.003	0.750 ± 0.120	0.090 ± 0.050
	NGC2168	8.250 ± 0.001	10.290 ± 0.010	-0.219 ± 0.015	0.774 ± 0.012	0.790 ± 0.040	0.100 ± 0.020
	NGC2477	9.019 ± 0.004	11.460 ± 0.000	-0.100 ± 0.000	0.750 ± 0.000	0.750 ± 0.030	0.070 ± 0.020
Cluster-specific Estimates	Hyades	8.785 ± 0.028	0.010 ± 0.030	0.164 ± 0.021	0.017 ± 0.006	0.650 ± 0.020	0.200 ± 0.060
	M67	9.591 ± 0.002	9.850 ± 0.010	-0.029 ± 0.007	0.142 ± 0.008	0.680 ± 0.010	0.050 ± 0.010
	NGC188	9.815 ± 0.002	11.510 ± 0.010	-0.056 ± 0.003	0.217 ± 0.003	4.520 ± 3.130	2.200 ± 1.750
	NGC2168	8.250 ± 0.001	10.290 ± 0.010	-0.221 ± 0.015	0.775 ± 0.012	0.810 ± 0.050	0.100 ± 0.020
	NGC2477	9.019 ± 0.004	11.460 ± 0.000	-0.100 ± 0.000	0.750 ± 0.000	0.760 ± 0.030	0.070 ± 0.020

chical model yields reasonable estimates for the IFMR parameters of NGC 188, $M_{\text{WD}} = 0.749 + 0.088(M_{\text{ZAMS}} - 3.0)$. For the other clusters, the hierarchical and cluster-specific estimates have slight differences due to the shrinkage effects of the hierarchical model, which are further illustrated in Fig. 7. The hierarchical and cluster-specific estimates of the IFMR slopes differ by about one standard deviation for both the Hyades and M67. This is caused by the shrinkage effect: IFMR slopes of the five clusters shrink their grand mean. M67 has the shallowest IFMR and the Hyades has the second steepest IFMR, shallower only than NGC 188, so they are more substantially affected by the hierarchical analysis.

Figs. 5 and 6 plot the colour magnitude diagrams (CMD) for the five clusters. Fig. 5 presents the U-V and B-V

CMDs for the Hyades and the rows of Fig. 6 display CMDs of clusters (from top to bottom) M67, NGC 188, NGC 2168, and NGC 2477. The solid (red) lines are from the hierarchical fits and the dashed (blue) lines are from the cluster-specific fits. In each row of Figs. 5 and 6, the left panel displays a close up of the WD region of the CMD and the right panel shows the MS/RG stars. The CMDs for the MS/RG regions from both the hierarchical and cluster-specific fits are similar for all five clusters. Likewise, the CMDs for the WDs are also similar, for all clusters except NGC 188. For NGC 188, the cluster-specific CMD (dashed blue) is quite far from the dimmest WD, while the hierarchical CMD (solid red) is consistent with all of the cluster's WDs. This illustrates an advantage of the hierarchical model.

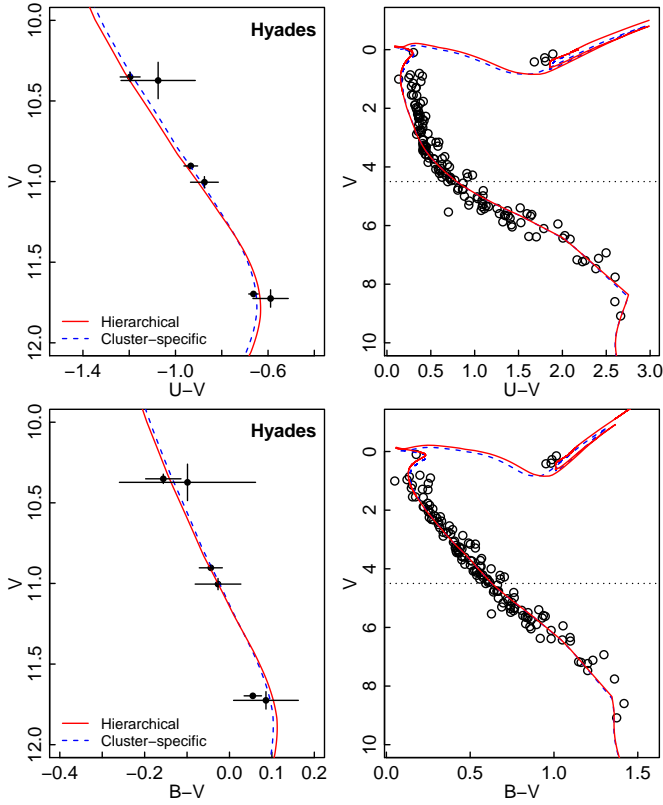


Figure 5. Color magnitude diagrams for the Hyades based on both the hierarchical and cluster-specific estimates. The solid (red) lines are from the hierarchical fits and dashed (blue) lines are from the cluster-specific fits.

Fig. 7 compares the estimated IFMRs (plotted as lines) for the five clusters along with the 68.3% contours (plotted as ovals) of the joint posterior distribution of initial (ZAMS) and final (WD) masses for each WD in each cluster. Results for both the hierarchical (solid) and cluster-specific (thick dashed) analyses are plotted. Colours (red, blue, green, purple, and black) correspond to five clusters (Hyades, M67, NGC 188, NGC 2168 and NGC 2477, respectively). The solid IFMR lines from the hierarchical fits tend to be in the centre and are consistent with the prior IFMRs (e.g. Williams, Bolte & Koester, 2004; Salaris et al. 2009; plotted as grey solid, dashed and dotted lines, respectively). The thick dashed fitted IFMRs from the cluster-specific approach have more uncertainty. The most striking feature of this figure is that the cluster-specific analysis of NGC 188 yields an unreasonably steep IFMR (plotted as a dashed green line), whereas the hierarchical model produces a much shallower

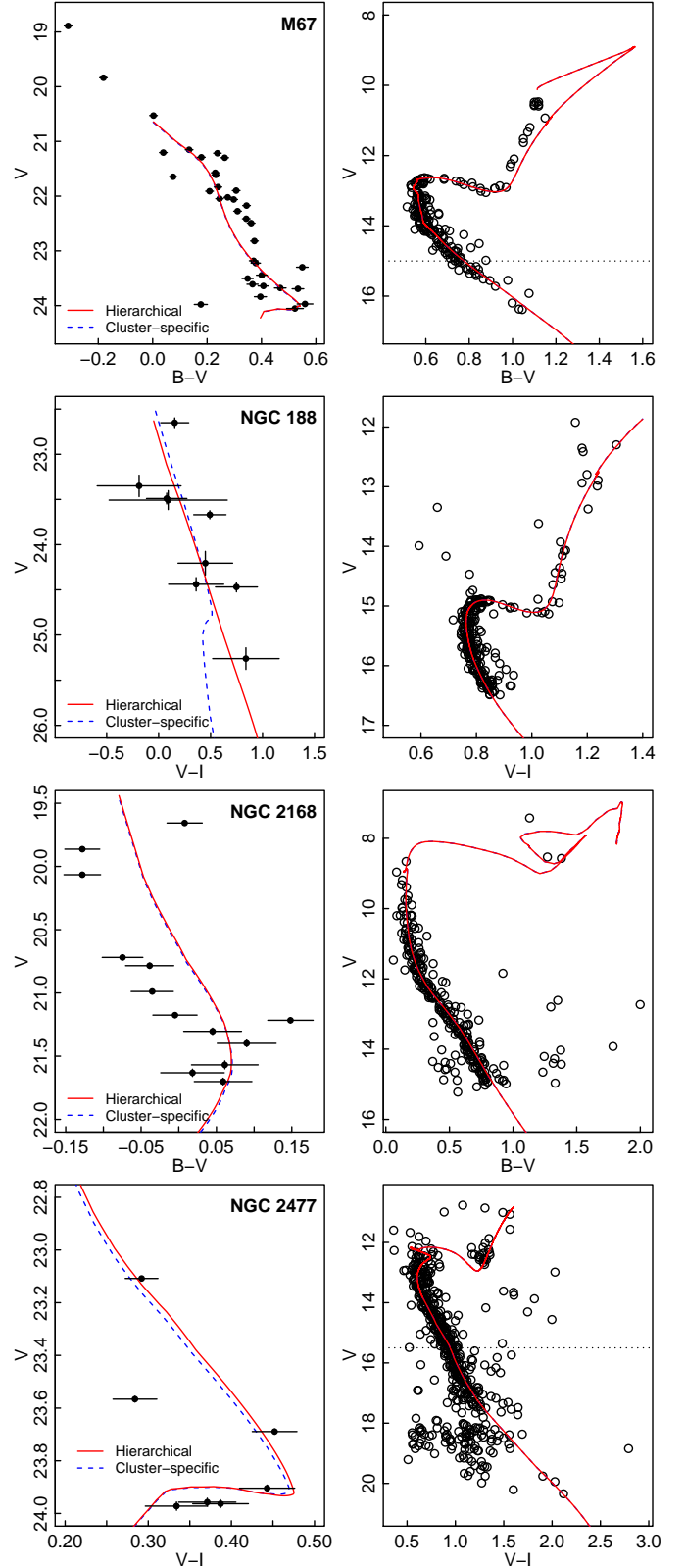


Figure 6. Color magnitude diagrams for (from top to bottom) M67, NGC 188, NGC 2168, NGC 2477, based on both the hierarchical and cluster-specific analyses. The solid (red) lines indicate the hierarchical fits and dashed (blue) lines indicate the cluster-specific fits.

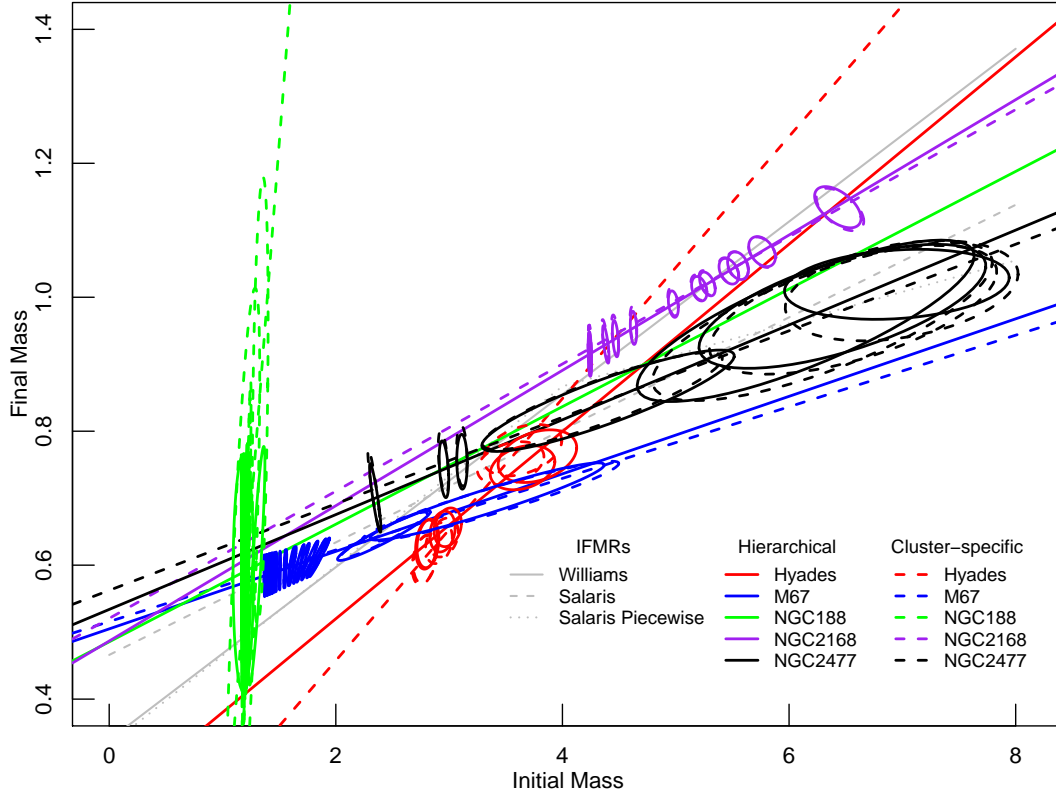


Figure 7. The estimated IFMRs for the five clusters obtained with both hierarchical and cluster-specific analyses. The ovals are 68.3% contours of the joint posterior distribution of the ZAMS and WD masses for the WDs in each cluster. The colour scheme of red, blue, green, purple, and black corresponds to the Hyades, M67, NGC 188, NGC 2168, and NGC 2477, respectively. The Williams, Salaris and Salaris piecewise IFMRs are plotted as solid, dashed, and dotted grey lines.

and more reasonable IFMR for NGC 188 (plotted as a solid green line).

Tables 9 — 11 present the initial masses, final masses, and membership probabilities for WDs in the five clusters, based on both the cluster-specific and hierarchical modelling approaches.

Table 12 presents the estimates of the average IFMR parameters under the Bayesian hierarchical model and compares them with results from Kalirai et al. (2008) and Williams et al. (2009). In our analysis, we include five clusters: the Hyades, M67, NGC 188, NGC 2168 and NGC 2477. The 68.3% credible intervals for the IFMR intercept and slope are 0.440 ± 0.140 (i.e., $[0.30, 0.58]$) and 0.090 ± 0.040 (i.e., $[0.05, 0.13]$), respectively. The point estimates of IFMR parameters from Kalirai et al. (2008) and Williams et al. (2009) falls into the credible intervals from our hierarchical model, so we consider that the average IFMR from our analysis is consistent with results from these studies.

The point estimate of IFMR intercept from our

Bayesian hierarchical analysis is 0.440, greater than intercepts from both Kalirai et al. (2008), 0.394, and Williams et al. (2009), 0.339. On the other hand, our estimate of the IFMR slope is the shallowest one, 0.090, and Williams et al. (2009) has the steepest IFMR, at 0.129.

The most obvious characteristic of our result lies in the large error bars, about 6 to 10 times the error bars in other analyses. There are three reasons for this. 1) Only five clusters are included in our analysis. By contrast, Kalirai et al. (2008) and Williams et al. (2009) employed 13 and 11 stellar clusters, respectively. They had more data to constrain the IFMR parameters, which leads to the narrow error bars in their studies. 2) In our analysis, clusters have different IFMR parameters and we report the mean IFMR of these clusters. However, Kalirai et al. (2008) and Williams et al. (2009) assume all clusters have the same IFMR. Their model is simpler and can be fit with fewer data. 3) Kalirai et al.

Table 9. Results from both the hierarchical and cluster-specific analyses for the WDs in the Hyades

Cluster	WD	Hierarchical Estimates			Cluster-specific Estimates		
		ZAMS Mass	WD Mass	Mem. Prob.	ZAMS Mass	WD Mass	Mem. Prob.
Hyades	HZ14	2.801 ± 0.064	0.631 ± 0.024	1.000	2.776 ± 0.067	0.607 ± 0.024	1.000
	VR16	2.813 ± 0.064	0.632 ± 0.024	1.000	2.787 ± 0.067	0.609 ± 0.024	1.000
	HZ7	2.942 ± 0.074	0.650 ± 0.020	1.000	2.910 ± 0.078	0.633 ± 0.020	1.000
	VR7	2.988 ± 0.079	0.657 ± 0.019	1.000	2.954 ± 0.084	0.641 ± 0.019	1.000
	HZ4	3.779 ± 0.229	0.763 ± 0.026	1.000	3.649 ± 0.228	0.772 ± 0.025	1.000
	LB227	3.648 ± 0.188	0.746 ± 0.022	1.000	3.543 ± 0.194	0.752 ± 0.021	1.000

Table 10. Results from the Hierarchical and Cluster-specific fits on WDs in M67

Cluster	WD	Hierarchical Estimates			Cluster-specific Estimates		
		ZAMS Mass	WD Mass	Mem. Prob.	ZAMS Mass	WD Mass	Mem. Prob.
M67	WD 1	1.615 ± 0.021	0.598 ± 0.019	1.000	1.619 ± 0.021	0.602 ± 0.017	1.000
	WD 2	1.438 ± 0.003	0.588 ± 0.020	1.000	1.438 ± 0.003	0.593 ± 0.018	1.000
	WD 3	1.429 ± 0.003	0.588 ± 0.020	1.000	1.429 ± 0.003	0.592 ± 0.018	1.000
	WD 4	1.412 ± 0.003	0.587 ± 0.020	0.000	1.412 ± 0.003	0.591 ± 0.018	0.000
	WD 5	1.364 ± 0.003	0.584 ± 0.021	0.209	1.364 ± 0.003	0.589 ± 0.019	0.191
	WD 6	1.426 ± 0.003	0.587 ± 0.020	1.000	1.426 ± 0.003	0.592 ± 0.018	1.000
	WD 7	1.414 ± 0.003	0.587 ± 0.020	1.000	1.414 ± 0.003	0.591 ± 0.018	1.000
	WD 8	1.396 ± 0.003	0.586 ± 0.020	1.000	1.395 ± 0.003	0.590 ± 0.018	1.000
	WD 9	1.389 ± 0.003	0.585 ± 0.020	1.000	1.388 ± 0.003	0.590 ± 0.018	1.000
	WD 10	1.556 ± 0.006	0.595 ± 0.019	1.000	1.558 ± 0.006	0.599 ± 0.017	1.000
	WD 11	1.431 ± 0.003	0.588 ± 0.020	0.983	1.431 ± 0.003	0.592 ± 0.018	0.981
	WD 12	1.394 ± 0.003	0.586 ± 0.020	0.329	1.393 ± 0.003	0.590 ± 0.018	0.253
	WD 13	1.370 ± 0.003	0.584 ± 0.021	1.000	1.370 ± 0.003	0.589 ± 0.018	1.000
	WD 14	1.506 ± 0.003	0.592 ± 0.019	0.999	1.507 ± 0.003	0.596 ± 0.017	0.999
	WD 15	1.454 ± 0.003	0.589 ± 0.020	1.000	1.454 ± 0.003	0.594 ± 0.018	1.000
	WD 16	1.828 ± 0.056	0.610 ± 0.019	1.000	1.838 ± 0.051	0.614 ± 0.017	1.000
	WD 17	1.440 ± 0.003	0.588 ± 0.020	1.000	1.440 ± 0.003	0.593 ± 0.018	1.000
	WD 18	1.473 ± 0.003	0.590 ± 0.019	0.595	1.473 ± 0.003	0.595 ± 0.017	0.544
	WD 19	1.549 ± 0.005	0.594 ± 0.019	1.000	1.550 ± 0.006	0.599 ± 0.017	1.000
	WD 20	1.389 ± 0.003	0.585 ± 0.020	0.173	1.388 ± 0.003	0.590 ± 0.018	0.221
	WD 21	1.363 ± 0.003	0.584 ± 0.021	0.033	1.363 ± 0.003	0.589 ± 0.019	0.030
	WD 22	2.424 ± 0.270	0.644 ± 0.025	1.000	2.424 ± 0.252	0.645 ± 0.023	1.000
	WD 23	3.335 ± 0.682	0.695 ± 0.038	1.000	3.365 ± 0.747	0.695 ± 0.040	1.000
	WD 24	1.398 ± 0.003	0.586 ± 0.020	0.092	1.398 ± 0.003	0.591 ± 0.018	0.056
	WD 25	1.671 ± 0.030	0.601 ± 0.019	0.999	1.677 ± 0.029	0.605 ± 0.017	1.000
	WD 26	1.768 ± 0.047	0.607 ± 0.019	1.000	1.777 ± 0.044	0.610 ± 0.017	1.000
	WD 27	1.466 ± 0.003	0.590 ± 0.020	0.976	1.466 ± 0.003	0.594 ± 0.018	0.971
	WD 28	1.708 ± 0.036	0.603 ± 0.019	1.000	1.715 ± 0.034	0.607 ± 0.017	1.000
	WD 29	1.607 ± 0.019	0.598 ± 0.019	1.000	1.611 ± 0.019	0.602 ± 0.017	1.000
	WD 30	1.812 ± 0.055	0.609 ± 0.019	0.000	1.822 ± 0.050	0.613 ± 0.017	0.000
	WD 31	1.437 ± 0.003	0.588 ± 0.020	1.000	1.437 ± 0.003	0.593 ± 0.018	1.000
	WD 32	1.856 ± 0.058	0.612 ± 0.019	0.996	1.867 ± 0.052	0.615 ± 0.017	0.998
	WD 33	1.412 ± 0.003	0.587 ± 0.020	1.000	1.412 ± 0.003	0.591 ± 0.018	1.000
	WD 34	1.449 ± 0.003	0.589 ± 0.020	0.098	1.449 ± 0.003	0.593 ± 0.018	0.073
	WD 35	1.599 ± 0.016	0.597 ± 0.019	0.093	1.602 ± 0.017	0.601 ± 0.017	0.060

(2008) and Williams et al. (2009) used linear regression to fit the initial and final masses of WDs in their clusters, so their estimates of the IFMR parameters are mainly subject to uncertainties of the WDs' initial and final masses. Their estimates are also indirectly affected by the ages and distances of clusters. However, we utilise a Bayesian hierarchical

model, which takes account of uncertainties of ages, distances, metallicities, etc.

4.3 Comparison with Spectroscopic Mass Estimates

In this section, we compare our estimates of initial and final masses of Hyades WDs with those deter-

Table 11. Results from the hierarchical and cluster-specific analyses for the WDs in NGC188, NGC2168 and NGC2477

Cluster	WD	Hierarchical Estimates			Cluster-specific Estimates		
		ZAMS Mass	WD Mass	Mem. Prob.	ZAMS Mass	WD Mass	Mem. Prob.
NGC188	WD 1	1.169 ± 0.003	0.588 ± 0.117	1.000	1.171 ± 0.003	0.510 ± 0.128	1.000
	WD 2	1.184 ± 0.003	0.590 ± 0.116	1.000	1.185 ± 0.003	0.538 ± 0.122	1.000
	WD 3	1.187 ± 0.002	0.590 ± 0.116	1.000	1.188 ± 0.002	0.544 ± 0.121	1.000
	WD 4	1.184 ± 0.060	0.590 ± 0.117	1.000	1.177 ± 0.100	0.519 ± 0.326	1.000
	WD 5	1.191 ± 0.002	0.590 ± 0.116	1.000	1.191 ± 0.002	0.551 ± 0.120	1.000
	WD 6	1.208 ± 0.006	0.592 ± 0.116	1.000	1.210 ± 0.010	0.595 ± 0.130	1.000
	WD 7	1.219 ± 0.009	0.592 ± 0.116	1.000	1.226 ± 0.017	0.639 ± 0.157	1.000
	WD 8	1.219 ± 0.009	0.592 ± 0.116	1.000	1.224 ± 0.015	0.628 ± 0.146	1.000
	WD 9	1.302 ± 0.048	0.599 ± 0.118	1.000	1.333 ± 0.046	0.845 ± 0.220	1.000
NGC2168	WD 1	4.627 ± 0.019	0.954 ± 0.016	1.000	4.625 ± 0.019	0.96 ± 0.017	1.000
	WD 2	5.762 ± 0.078	1.068 ± 0.015	1.000	5.764 ± 0.079	1.067 ± 0.015	1.000
	WD 3	5.279 ± 0.045	1.020 ± 0.012	1.000	5.277 ± 0.047	1.021 ± 0.012	1.000
	WD 4	4.244 ± 0.008	0.916 ± 0.022	1.000	4.243 ± 0.008	0.923 ± 0.023	1.000
	WD 5	4.240 ± 0.008	0.915 ± 0.022	1.000	4.239 ± 0.008	0.923 ± 0.023	1.000
	WD 6	5.208 ± 0.045	1.013 ± 0.012	1.000	5.203 ± 0.046	1.015 ± 0.013	1.000
	WD 7	6.430 ± 0.135	1.134 ± 0.020	1.000	6.450 ± 0.138	1.131 ± 0.021	1.000
	WD 8	4.468 ± 0.018	0.938 ± 0.018	1.000	4.465 ± 0.020	0.945 ± 0.019	1.000
	WD 9	4.240 ± 0.008	0.915 ± 0.022	1.000	4.239 ± 0.008	0.923 ± 0.023	1.000
	WD 10	5.469 ± 0.057	1.039 ± 0.013	1.000	5.467 ± 0.059	1.039 ± 0.013	1.000
	WD 11	5.549 ± 0.061	1.047 ± 0.014	1.000	5.546 ± 0.062	1.047 ± 0.014	1.000
	WD 12	4.383 ± 0.019	0.930 ± 0.019	1.000	4.378 ± 0.020	0.936 ± 0.020	1.000
	WD 13	4.979 ± 0.029	0.990 ± 0.013	1.000	4.976 ± 0.030	0.993 ± 0.014	1.000
NGC2477	WD 1	2.348 ± 0.033	0.701 ± 0.034	1.000	2.337 ± 0.036	0.714 ± 0.040	1.000
	WD 2	3.114 ± 0.031	0.754 ± 0.027	1.000	3.112 ± 0.031	0.763 ± 0.030	1.000
	WD 3	2.954 ± 0.028	0.743 ± 0.028	0.950	2.949 ± 0.030	0.753 ± 0.031	0.964
	WD 4	6.951 ± 0.654	1.019 ± 0.034	1.000	6.994 ± 0.678	1.010 ± 0.049	1.000
	WD 5	6.471 ± 0.835	0.986 ± 0.061	1.000	6.565 ± 0.836	0.981 ± 0.063	1.000
	WD 6	6.147 ± 0.981	0.965 ± 0.080	1.000	6.294 ± 0.990	0.964 ± 0.078	1.000
	WD 7	4.402 ± 0.735	0.845 ± 0.050	1.000	4.354 ± 0.698	0.845 ± 0.048	1.000

Table 12. Estimates of the average IFMR parameters from the hierarchical model and comparisons with other results

	IFMR Intercept	IFMR Slope
Hierarchical Model	0.440 ± 0.140	0.090 ± 0.040
Kalirai et al. (2008)	0.394 ± 0.025	0.109 ± 0.007
Williams et al. (2009)	0.339 ± 0.015	0.129 ± 0.004

mined spectroscopically by Kalirai et al. (2014). The meaningful comparison is among the final masses of WDs, because that is what Kalirai et al. are directly determining with their spectroscopy.

Table 13 and Fig. 8 present the 68.3% confidence intervals (CIs) for these initial and final WD masses. The left panel presents the initial masses and the right panel presents the final masses. In each of these plots, bars parallel to the x-axis and y-axis are 68.3% CIs from our hierarchical analysis and Kalirai et al. (2014), respectively. The BASE-9 results in Fig. 8 are ~ 0.05 to $0.10M_{\odot}$ lower than the spectroscopic re-

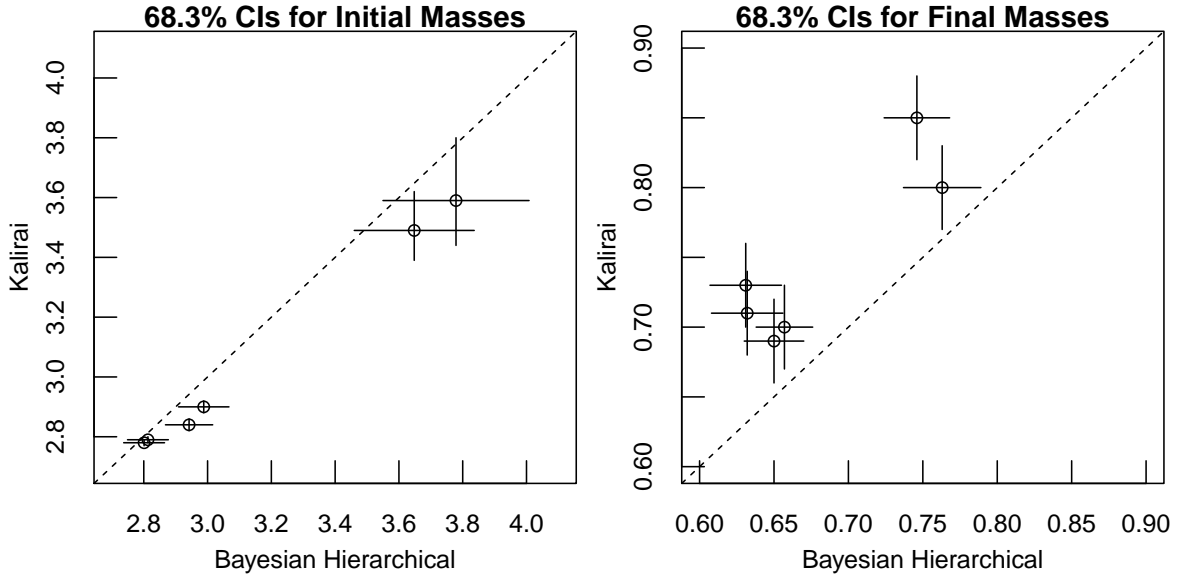
sults from Kalirai et al.. Interestingly, both are ultimately based on the Montreal white dwarf group's models, though the spectroscopic technique relies on the Balmer line profiles whereas the photometric technique relies on the overall SED of the WD. While these differences are small, at least in this case they appear systematic, and may indicate subtle inconsistencies between the model colours and line profiles. Alternatively, the photometric technique relies on the cluster distance, which may be slightly in error and will be improved upon in the near future with Gaia results.

5 SENSITIVITY ANALYSIS

In this section, we present the sensitivity analysis in the hierarchical analysis of IFMR parameters.

Table 13. 68.3% confidence intervals for the initial and final masses of WDs in Hyades obtained through our hierarchical model and spectroscopic analysis in Kalirai et al. (2014)

WDs	Name	Initial Mass		Final Mass	
		Hierarchical	Kalirai et al.	Hierarchical	Kalirai et al.
0352+096	HZ 4	3.779 ± 0.229	$3.59^{+0.21}_{-0.15}$	0.763 ± 0.026	0.80 ± 0.03
0406+169	LB 227	3.648 ± 0.188	$3.49^{+0.13}_{-0.10}$	0.746 ± 0.022	0.85 ± 0.03
0421+162	VR 7	2.988 ± 0.079	2.90 ± 0.02	0.657 ± 0.019	0.70 ± 0.03
0425+168	VR 16	2.813 ± 0.064	2.79 ± 0.01	0.632 ± 0.024	0.71 ± 0.03
0431+126	HZ 7	2.942 ± 0.074	2.84 ± 0.02	0.650 ± 0.020	0.69 ± 0.03
0438+108	HZ 14	2.801 ± 0.064	2.78 ± 0.01	0.631 ± 0.024	0.73 ± 0.03

**Figure 8.** The 68.3% confidence intervals for initial and final masses of the Hyades WDs from our Bayesian hierarchical modelling and Kalirai et al. (2014). The left panel compares the initial masses of the two approaches and the right panel compares the final masses. Horizontal and vertical error bars represents the 68.3% CIs from our hierarchical analysis and Kalirai et al. (2014).

5.1 Sensitivity to Prior Distribution

Here we investigate whether the hierarchical analysis in Eq. 6 is sensitive to the prior distribution on Γ . We use the marginally non-informative prior distribution proposed by Huang & Wand (2013), i.e.,

$$\Gamma \mid \lambda_1, \lambda_2 \sim \text{Inverse Wishart} \left(2\nu \begin{pmatrix} 1/\lambda_1 & 0 \\ 0 & 1/\lambda_2 \end{pmatrix}, \nu + 1 \right),$$

$$\lambda_1, \lambda_2 \sim \text{Inverse Gamma}(1/2, 1/\Lambda),$$

λ_1 and λ_2 are hyper-parameters, and they independently follow the same inverse gamma distribution with its first parameter fixed at $1/2$ and second parameter $1/\Lambda$ a small positive number, i.e., large positive Λ . Huang & Wand (2013) showed that $\nu = 2$ leads to a marginal uniform distribution for correlation ρ and arbitrarily large positive Λ leads

to arbitrarily weakly informative prior distributions for σ_1 and σ_2 . Because $\nu = 2$ is necessary to have a marginally non-informative prior distribution on ρ , so in this hierarchical analysis, we take $\nu = 2$. As for Λ , we choose four large values: $10^3, 10^4, 10^5, 10^6$ and fit the hierarchical model with these values, then compare the MCMC draws of IFMR parameters of the five included clusters.

Figs 9–11 present the QQ plots of IFMR parameters from the hierarchical fits when Λ takes different values. All points in these QQ plots lie close to the 45° red line, meaning that MCMC draws of IFMR parameters are essentially the same. Though there are some small deviations from the red line, they are mainly caused by Monte Carlo errors. So we conclude that the hierarchical result is not sensitive to the choice of value of Λ provided that $\Lambda \geq 10^3$.

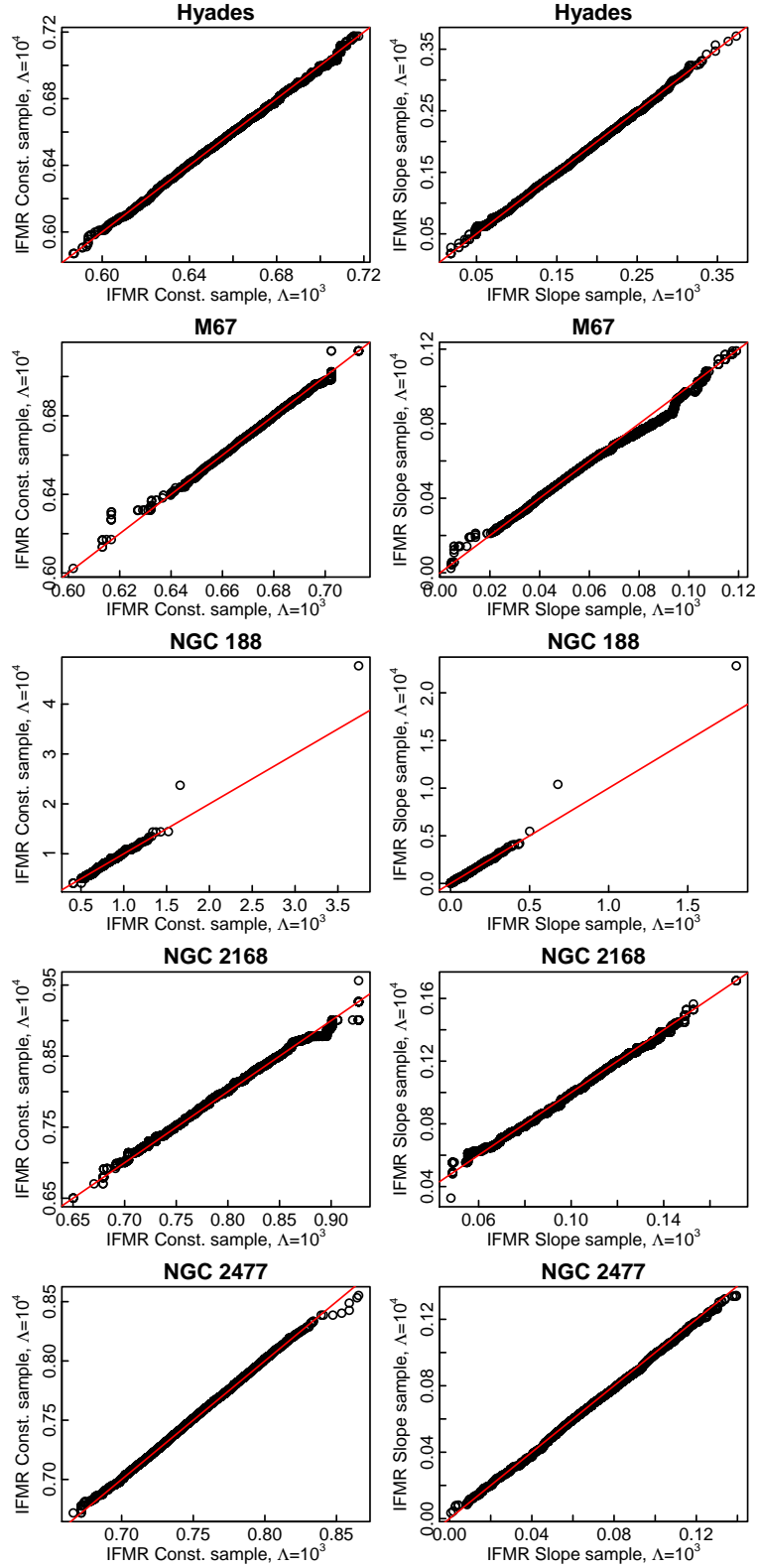


Figure 9. Quantile-quantile plots of MCMC samples of IFMR parameters of five clusters. The x-axis and y-axis are quantiles corresponding to fits with $\Lambda = 10^3$ and $\Lambda = 10^4$, respectively. The 45° red line represents that quantiles from samples in x and y axes are equal.

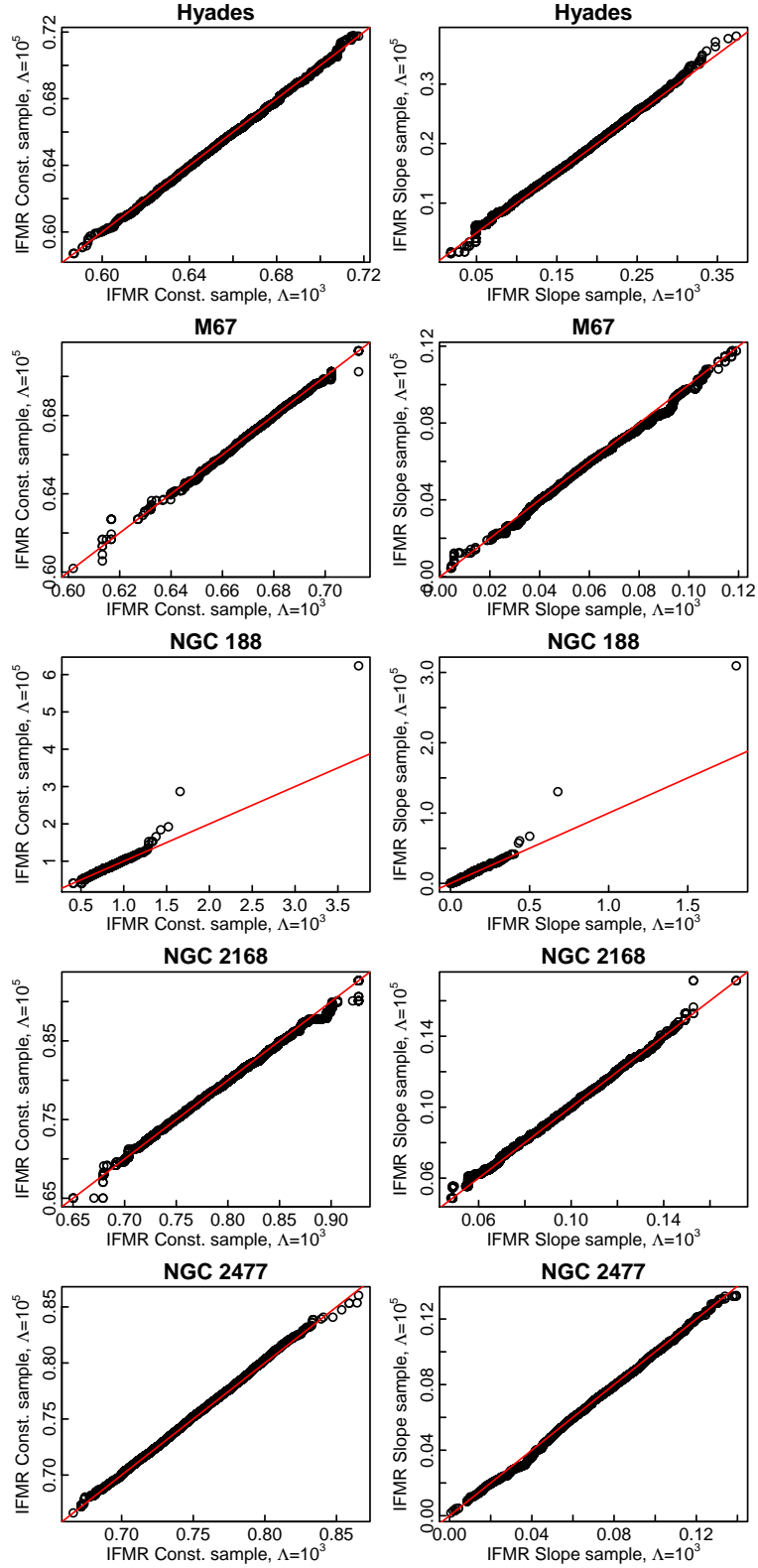


Figure 10. Quantile-quantile plots of MCMC samples of IFMR parameters of five clusters. The x-axis and y-axis are quantiles corresponding to fits with $\Lambda = 10^3$ and $\Lambda = 10^5$, respectively. The 45° red line represents that quantiles from samples in x and y axes are equal.

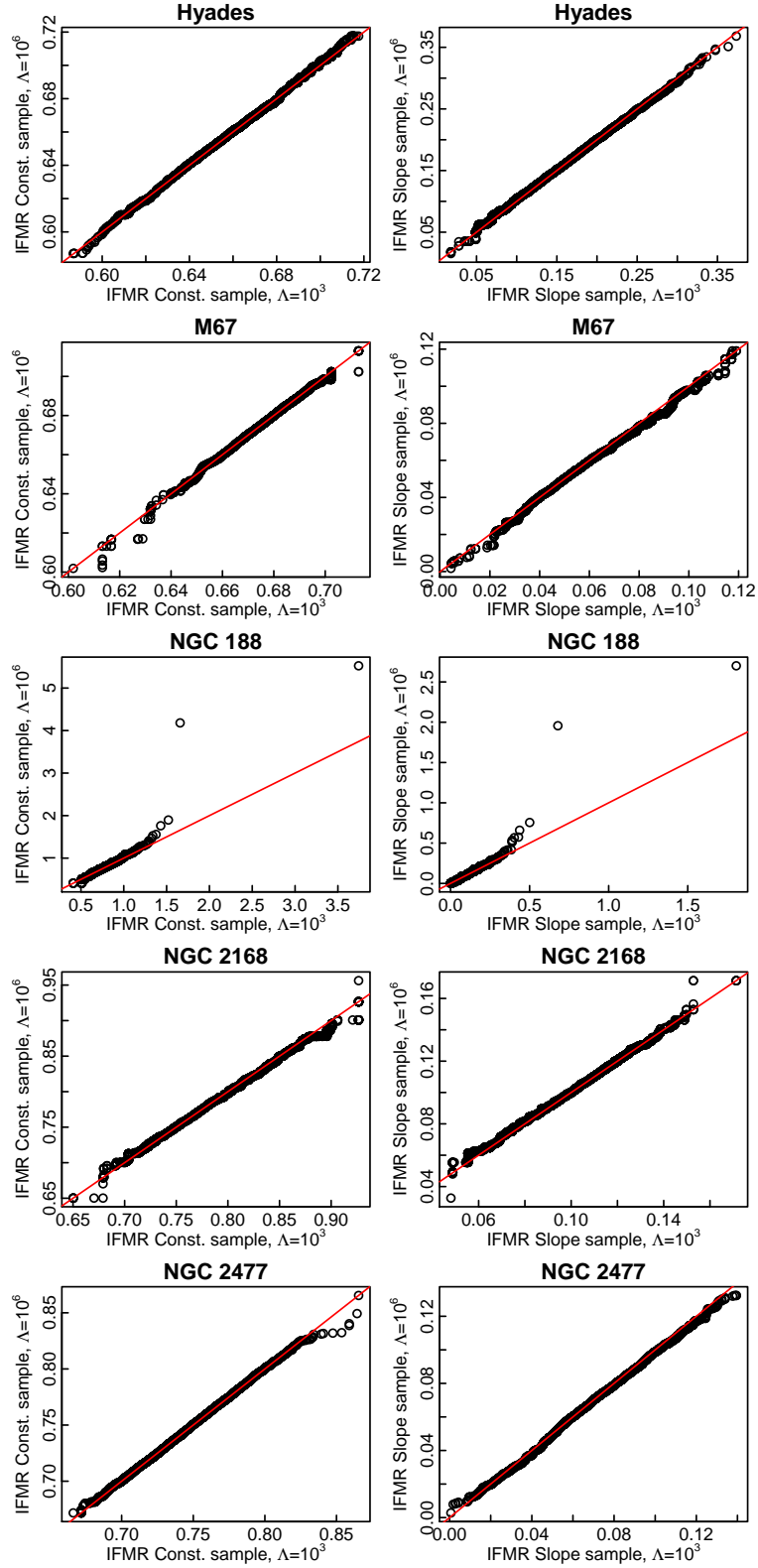


Figure 11. Quantile-quantile plots of MCMC samples of IFMR parameters of five clusters. The x-axis and y-axis are quantiles corresponding to fits with $\Lambda = 10^3$ and $\Lambda = 10^6$, respectively. The 45° red line represents that quantiles from samples in x and y axes are equal.

5.2 Sensitivity to Membership of WDs in M67

Table 10 presents the hierarchical and case-by-case estimates of initial and final masses and membership probabilities for 35 WDs in M67, among which nine WDs have posterior membership probabilities less than 0.5 and are classified as non-members or field stars. The other 26 WDs are inferred as members of M67. In this section we investigate whether the membership of these nine WDs affects the case-by-case posterior distribution of cluster M67.

In Section 4, when performing the case-by-case analysis on the cluster M67 with BASE-9, we set the prior membership probabilities of all WDs based on other research (e.g., Bellini et al. 2010a,b; Williams et al. 2013; Barnes et al. 2016). For clarity, we call this analysis the original fit. Then we fit M67 under two other circumstances: 1.) Case I: setting all WDs to have a 100% prior probability of being a member in M67, and 2.) Case II: assigning nine non-members as determined by the original fit (Table 10) to have prior membership probabilities equal to 0 and the apparent cluster members to have prior probabilities equal to 1. In other words, the first case forces all WDs in M67 to be cluster members whereas the second case removes nine apparent non-members and assumes that the other 26 as definitive cluster members.

Table 14 presents the point estimates of M67 parameters under three settings. The last two columns present the IFMR constant and slope, respectively. The case-by-case estimates of the IFMR slope vary under different settings. In Case I, when all WDs are forced to be M67 members, the IFMR slope is the steepest, while in the original fit, the IFMR is the shallowest. The estimates of other parameters are similar under the settings except the age. The estimate of age from the original fit is consistent to that from the Case II, while the age estimate from Case I is younger than the others. The age estimates from the original fit and Case I are close to the results obtained through other approaches (Bellini et al. 2010b; Williams et al. 2013).

Fig. 12 presents the CMD plots for these three fits. The black lines are from the fitted model under the original fit, and the red and blue lines are from models under Case I and II, respectively. From this plot, both fits from Case I

(red line) and II (blue line) miss the main sequence turnoff stars, sub-giant branch and base of the red giant branch. By contrast, the model under the original fit (black line) matches both parts of the cluster well. We conclude that the original fit, where BASE-9 was able to assign its own cluster membership probabilities, is more reliable than the other fits. In summary, the membership of these WDs affect the posterior distribution of cluster parameters, yet our further analysis supports the original fit because it best matches the photometric data among those three fits.

5.3 Sensitivity to WD-WD Binaries

Our BASE-9 model does not include WD-WD binaries. While it will likely be preferable to do so eventually, current studies of cluster WDs are inadequate to determine the fraction of double degenerates in clusters and even further from determining which cluster WDs are unresolved binaries. The possible exceptions to this are the Hyades WDs, which are nearby, relatively bright, and well-studied. Among the 7 Hyades in our study, it is likely that all are single WDs. Theoretical studies (e.g., Hurley et al. 2005) indicate that the number of unresolved WD-WD binaries is probably $< 10\%$ of a cluster's WD population. Thus ~ 3 of the M67 WDs and ~ 1 each for NGC 188, NGC 2168, and NGC 2477 may be unresolved double degenerates. The WD regions of the CMDs for all of these clusters are consistent with this possibility. Fortunately, BASE-9 is robust against a small fraction of WDs having a large effect on the IFMR fit because (a) the double degenerate fraction is likely to be small and (b) objects that fall overly far from the best fit isochrones are fit as non-members and therefore do not contribute to the cluster solution (age, WD mass, IFMR parameters).

6 CONCLUSIONS AND DISCUSSIONS

We proposed a Bayesian hierarchical model for the IFMR parameters that simultaneously analyses data from multiple clusters in a single overall model and produces more precise

Table 14. Estimated cluster parameters for M67 under three cases.

Settings	Age (Gyr)	$m - M_V$	[Fe/H] ¹	Abs. ¹	IFMR Constant	IFMR Slope
Original	3.90 ± 0.02	9.85 ± 0.01	-0.03	0.14	0.68 ± 0.01	0.05 ± 0.01
Case I	3.07 ± 0.03	9.86 ± 0.02	-0.01	0.15	0.67 ± 0.01	0.10 ± 0.01
Case II	3.89 ± 0.02	9.86 ± 0.01	-0.04	0.16	0.68 ± 0.01	0.07 ± 0.01

¹: The standard errors for metallicity and absorption under these fits are all 0.01.

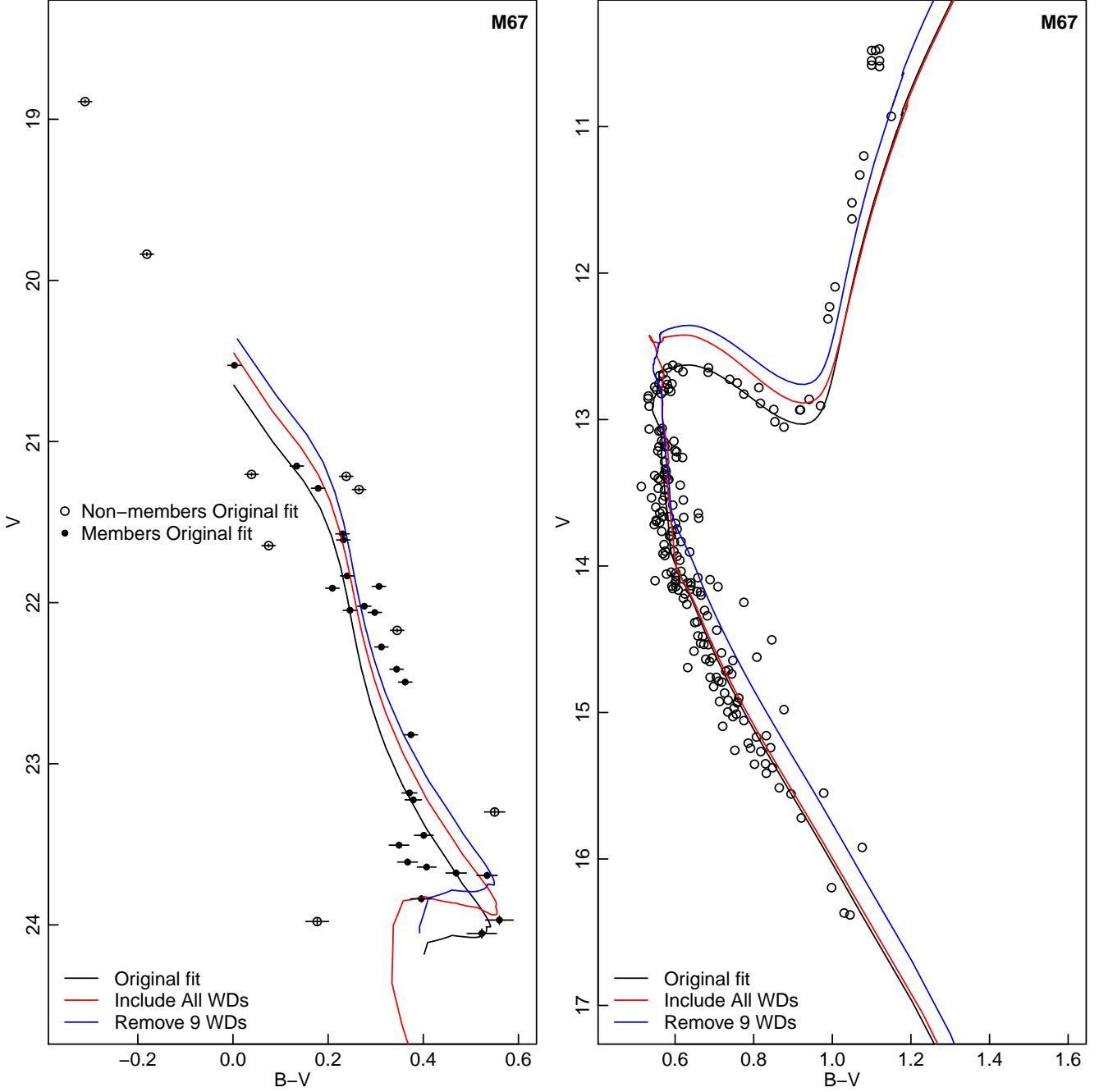


Figure 12. Colour-magnitude diagram (CMD) plots of three fits. The black lines are from the original fit, red lines from the fit that includes all WDs in M67, blue lines from the fit that removes nine non-members. In the left panel, open circles represent non-member WDs from the original fit and solid points are members. Observed error bars are included for the WDs.

estimates of the IFMR parameters. Also, we develop an efficient two-stage algorithm that takes advantage of existing software for cluster-specific analysis to obtain the fit under the hierarchical model. We combine data from five open clusters in the Bayesian hierarchical model and find that it can correct an error in the estimates of IFMR parameters for the cluster NGC 188 and produce reasonable estimates of IFMR for NGC 188. Based on our hierarchical analysis, we estimate the linear IFMR averaged across clusters to be

$$M_{\text{final}} = (0.09 \pm 0.04)M_{\text{initial}} + (0.44 \pm 0.14)M_{\odot},$$

with $0.8M_{\odot} \leq M_{\text{initial}} \leq 8.0M_{\odot}$.

This paper focus on the use of statistical techniques to the IFMR project, and the detailed results are preliminary. In particular, the astronomical results in this paper are not definitive and they depend upon the models inside the black-box code (in our case, the BASE-9) and other assumptions. Specifically, we assumed that the IFMR parameters from different clusters follow a bivariate normal distribution. However, this assumption might be too idealised. Bayesian hierarchical models always require a population distribution on all objects and the shape of the distribution of IFMR parameters across all clusters is not available. We therefore use the bivariate normal distribution as a starting point. If a case can be made for a different distribution, the statistical algorithm developed in this chapter will work as long as the case-by-case results are valid. Studies have indicated that metallicity may affect the IFMR (See, e.g., [Kalirai et al. 2005](#); [Catalan et al. 2008](#); [Meng et al. 2008](#); [Zhao et al. 2012](#)). We showed how the Bayesian hierarchical model in Eq. (6) can be readily extended to investigate the effect of metallicity. **In addition, even though our research is based on the BASE-9 package, our statistical techniques can be employed with other black-box packages as long as they produce MCMC samples in their case-by-case fits. Different underlying stellar evolution models will affect the results of case-by-case fits, hence they will most likely impact the resulting hierarchical fit. Our statistical approach and computational algorithm are independent of these inputs and can be broadly applied.**

ACKNOWLEDGEMENTS

We thank the Imperial College High Performance Computing support team for their kind help, which greatly accelerated the simulation study in this project. Shijing Si thanks the Department of Mathematics in Imperial College London for a Roth studentship, which supported his research. David van Dyk acknowledges support from a Marie-Skłodowska-Curie RISE Grant (H2020-MSCA-RISE-2015-691164) provided by the European Commission. Ted von Hippel acknowledges support from the National Science Foundation under Award AST-1715718.

REFERENCES

- Andrews J. J., Agüeros M. A., Gianninas A., Kilic M., Dhital S., Anderson S. F., 2015, *Astrophysical Journal*, 815, 63
- Barnes S. A., Weingrill J., Fritzewski D., Strassmeier K. G., Platais I., 2016, *Astrophysical Journal*, 823, 16
- Bellini A., Bedin L., Pichardo B., Moreno E., Allen C., Piotto G., Anderson J., 2010a, *Astronomy and Astrophysics*, 513, 51
- Bellini A., et al., 2010b, *Astronomy and Astrophysics*, 513, 50
- Bergeron P., Wesemael F., Beauchamp A., 1995, *Publications of the Astronomical Society of the Pacific*, 107, 1047
- Browne W., Goldstein H., 2002, Technical report, An Introduction to Bayesian Multilevel Hierarchical Modelling using MLwiN. Institute of Education, London
- Browne W. J., Draper D., et al., 2006, *Bayesian analysis*, 1, 473
- Catalan S., Isern J., García-Berro E., Ribas I., 2008, *Monthly Notices of the Royal Astronomical Society*, 387, 1693
- Choi J., Dotter A., Conroy C., Cantiello M., Paxton B., Johnson B. D., 2016, *Astrophysical Journal*, 823, 102
- Clopper C. J., Pearson E. S., 1934, *Biometrika*, 26, 404
- Cummings J. D., Kalirai J. S., Tremblay P.-E., Ramirez-Ruiz E., 2016, *Astrophysical Journal*, 818, 84
- DeGennaro S., 2009, PhD thesis, The University of Texas at Austin
- DeGennaro S., von Hippel T., Jefferys W. H., Stein N., van Dyk D., Jeffery E., 2009, *Astrophysical Journal*, 696, 12
- Dotter A., Chaboyer B., Jevremović D., Kostov V., Baron E., Ferguson J. W., 2008, *Astrophysical Journal Supplement Series*, 178, 89
- Gelman A., 2006, *Technometrics*, 48, 241
- Gelman A., Carlin J. B., Stern H. S., Rubin D. B., 2013, *Bayesian data analysis*. Chapman & Hall/CRC Texts in Statistical Science Vol. 3, Taylor & Francis

Girardi L., Bressan A., Bertelli G., Chiosi C., 2000, *Astronomy and Astrophysics Supplement Series*, 141, 371

Huang A., Wand M. P., 2013, *Bayesian Analysis*, 8, 439

Hurley J. R., Pols O. R., Aarseth S. J., Tout C. A., 2005, *Monthly Notices of the Royal Astronomical Society*, 363, 293

Jeffery E. J., von Hippel T., DeGennaro S., van Dyk D. A., Stein N., Jefferys W. H., 2011, *Astrophysical Journal*, 730, 35

Jiao X., van Dyk D. A., Trotta R., Shariff H., 2016, *The Efficiency of Next-Generation Gibbs-Type Samplers: An Illustration Using a Hierarchical Model in Cosmology*. Springer

Kalirai J. S., Richer H. B., Reitzel D., Hansen B. M., Rich R. M., Fahlman G. G., Gibson B. K., von Hippel T., 2005, *Astrophysical Journal*, 618, L123

Kalirai J. S., Hansen B. M., Kelson D. D., Reitzel D. B., Rich R. M., Richer H. B., 2008, *Astrophysical Journal*, 676, 594

Kalirai J. S., Marigo P., Tremblay P.-E., 2014, *Astrophysical Journal*, 782, 17

Mandel K. S., Scolnic D. M., Shariff H., Foley R. J., Kirshner R. P., 2017, *Astrophysical Journal*, 842, 93

Marigo, P. Girardi, L. 2007, *Astronomy & Astrophysics*, 469, 239

Meibom S., et al., 2009, *Astronomical Journal*, 137, 5086

Meng X., Chen X., Han Z., 2008, *Astronomy and Astrophysics*, 487, 625

Miller G. E., Scalo J. M., 1979, *Astrophysical Journal Supplement Series*, 41, 513

Montgomery M., Klumpe E., Winget D., Wood M., 1999, *Astrophysical Journal*, 525, 482

Morris C. N., Lysy M., 2012, *Statistical Science*, 27, 115

Perryman M. A. C., et al., 1998, *Astronomy and Astrophysics*, 331, 81

R Core Team 2017, *R: A Language and Environment for Statistical Computing*. R Foundation for Statistical Computing, Vienna, Austria, <https://www.R-project.org/>

Salaris M., Serenelli A., Weiss A., Bertolami M. M., 2009, *Astrophysical Journal*, 692, 1013

Shariff H., Jiao X., Trotta R., van Dyk D. A., 2016, *Astrophysical Journal*, 827, 1

Si S., van Dyk D. A., 2018, *Simple Two-Stage Algorithms for Fitting Hierarchies of Complex Models*, In preparation

Si S., van Dyk D. A., von Hippel T., Robinson E., Webster A., Stenning D., 2017a, *Monthly Notices of the Royal Astronomical Society*, 468, 4374

Si S., van Dyk D. A., von Hippel T., 2017b, in Tremblay P.-E., Gaensicke B., Marsh T., eds, *Astronomical Society of the Pacific Conference Series Vol. 509, 20th European White Dwarf*

Workshop. pp 69–72

Stein N. M., van Dyk D. A., von Hippel T., DeGennaro S., Jeffery E. J., Jefferys W. H., 2013, *Statistical Analysis and Data Mining: The ASA Data Science Journal*, 6, 34

Stenning D., Wagner-Kaiser R., Robinson E., Van Dyk D., Von Hippel T., Sarajedini A., Stein N., 2016, *Astrophysical Journal*, 826, 41

Sung H., Bessell M., 1999, *Monthly Notices of the Royal Astronomical Society*, 306, 361

Taylor B., 2006, *Astronomical Journal*, 133, 370

VandenBerg D. A., Stetson P., 2004, *Publications of the Astronomical Society of the Pacific*, 116, 997

Williams K. A., Bolte M., Koester D., 2004, *Astrophysical Journal Letters*, 615, L49

Williams K. A., Bolte M., Koester D., 2009, *Astrophysical Journal*, 693, 355

Williams K. A., Howell S. B., Liebert J., Smith P. S., Bellini A., Rubin K. H., Bolte M., 2013, *Astronomical Journal*, 145, 129

Zhao J. K., Oswalt T. D., Willson L. A., Wang Q., Zhao G., 2012, *Astrophysical Journal*, 746, 144

de Bruijne, J. H. J. Hoogerwerf, R. de Zeeuw, P. T. 2001, *Astronomy & Astrophysics*, 367, 111

van Dyk D. A., Park T., 2008, *Journal of the American Statistical Association*, 103, 790

van Dyk D. A., Degennaro S., Stein N., Jefferys W. H., von Hippel T., 2009, *Annals of Applied Statistics*, 3, 117

von Hippel T., Sarajedini A., 1998, *Astronomical Journal*, 116, 1789

von Hippel T., Jefferys W. H., Scott J., Stein N., Winget D., DeGennaro S., Dam A., Jeffery E., 2006, *Astrophysical Journal*, 645, 1436

von Hippel T., et al., 2014, *arXiv preprint arXiv:1411.3786*

APPENDIX A: COMPUTATIONAL ALGORITHM

The joint posterior distribution in Eq. 7 is high-dimensional, with $2N \times K + 6K + 7$ parameters. In this appendix, we show how to take advantage of the cluster-specific fittings in BASE-9 via a two-stage (TS) algorithm to fit the hierarchical model.

To simplify the description of the TS algorithm, we introduce $\mathbf{\Omega}_k = (\mathbf{M}_k, \mathbf{R}_k, \mathbf{Z}_k, \mathbf{\Theta}_k)$ for $k = 1, 2, \dots, K$. We use $\mathbf{\Psi} = \text{diag}(1/\lambda_1, 1/\lambda_2)$.

Step 0a: For each star cluster run BASE-9 to obtain a Monte Carlo sample of $p(\mathbf{M}_k, \mathbf{R}_k, \boldsymbol{\alpha}_k, \mathbf{Z}_k, \boldsymbol{\Theta}_k | \mathbf{X}_k, \boldsymbol{\Sigma}_k)$ via the cluster-specific analysis. Thin each chain to obtain an essentially independent Monte Carlo sample and label it $\{\boldsymbol{\Omega}_1^{(t)}, \boldsymbol{\alpha}_1^{(t)}, \dots, \boldsymbol{\Omega}_K^{(t)}, \boldsymbol{\alpha}_K^{(t)}, t = 1, 2, \dots, t_{MC}\}$.

Step 0b: In the following, we denote the TS samples with the tilde notation. Simulate K random integers between 1 and t_{MC} , denote them r_1^*, \dots, r_K^* , and initialise the parameters $\tilde{\boldsymbol{\alpha}}_k^{(1)} = \boldsymbol{\alpha}_k^{(r_k^*)}$ and $\tilde{\boldsymbol{\Omega}}_k^{(1)} = \boldsymbol{\Omega}_k^{(r_k^*)}$ for $k = 1, \dots, K$.

Step 0c: Given $\tilde{\boldsymbol{\Omega}}_1^{(1)}, \tilde{\boldsymbol{\alpha}}_1^{(1)}, \dots, \tilde{\boldsymbol{\Omega}}_K^{(1)}, \tilde{\boldsymbol{\alpha}}_K^{(1)}$, simulate $\tilde{\boldsymbol{\gamma}}^{(1)}$ and $\tilde{\boldsymbol{\Gamma}}^{(1)}$ via the partially collapsed Gibbs (PCG) sampler (van Dyk & Park 2008),

$$\tilde{\boldsymbol{\Gamma}}^{(1)} \sim \text{Inverse Wishart}\left(K + \nu, \sum_{k=1}^K (\tilde{\boldsymbol{\alpha}}_k^{(1)} - \tilde{\boldsymbol{\alpha}}^{(1)})(\tilde{\boldsymbol{\alpha}}_k^{(1)} - \tilde{\boldsymbol{\alpha}}^{(1)})^\top\right),$$

$$\tilde{\boldsymbol{\gamma}}^{(1)} \sim \text{N}_2\left(\tilde{\boldsymbol{\alpha}}^{(1)}, \tilde{\boldsymbol{\Gamma}}^{(1)}/K\right),$$

with $\tilde{\boldsymbol{\alpha}}^{(1)} = \frac{1}{K} \sum_{k=1}^K \tilde{\boldsymbol{\alpha}}_k^{(1)}$.

Step 0d: Given $\tilde{\boldsymbol{\Gamma}}^{(1)}$, we simulate λ_1, λ_2 from their conditional posterior distributions,

$$\tilde{\lambda}_\ell^{(1)} \sim \text{Inverse Gamma}\left(1 + \nu/2, \frac{1}{\Lambda_\ell} + \nu(\tilde{\boldsymbol{\Gamma}}^{(1)})_{\ell\ell}^{-1}\right)$$

for $\ell = 1, 2$.

For $s = 1, \dots$, run Step 1 and Step 2 iteratively.

Step 1: Randomly generate K integers between 1 and t_{MC} , and denote them r_1, \dots, r_K . For each $k = 1, \dots, K$, set $\boldsymbol{\alpha}_k^* = \boldsymbol{\alpha}_k^{(r_k)}$ and $\boldsymbol{\Omega}_k^* = \boldsymbol{\Omega}_k^{(r_k)}$ as the new proposal and set $\tilde{\boldsymbol{\alpha}}_k^{(s+1)} = \boldsymbol{\alpha}_k^*$, $\tilde{\boldsymbol{\Omega}}_k^{(s+1)} = \boldsymbol{\Omega}_k^*$ with probability $\min\left\{1, \frac{p(\boldsymbol{\alpha}_k^* | \tilde{\boldsymbol{\gamma}}^{(s)}, \tilde{\boldsymbol{\Gamma}}^{(s)})}{p(\boldsymbol{\alpha}_k^{(s)} | \tilde{\boldsymbol{\gamma}}^{(s)}, \tilde{\boldsymbol{\Gamma}}^{(s)})}\right\}$. Otherwise, set $\tilde{\boldsymbol{\alpha}}_k^{(s+1)} = \tilde{\boldsymbol{\alpha}}_k^{(s)}$, $\tilde{\boldsymbol{\Omega}}_k^{(s+1)} = \tilde{\boldsymbol{\Omega}}_k^{(s)}$.

Step 2: Given $\tilde{\lambda}_\ell^{(s)}, \ell = 1, 2$ and $\tilde{\boldsymbol{\alpha}}_k^{(s+1)}$, and $\tilde{\boldsymbol{\Omega}}_k^{(s+1)}, k = 1, \dots, K$, update $\tilde{\boldsymbol{\gamma}}, \tilde{\boldsymbol{\Gamma}}$ via

$$\tilde{\boldsymbol{\Gamma}}^{(s+1)} \sim \text{Inverse Wishart}\left(K + \nu, \sum_{k=1}^K (\tilde{\boldsymbol{\alpha}}_k^{(s+1)} - \tilde{\boldsymbol{\alpha}}^{(s+1)})(\tilde{\boldsymbol{\alpha}}_k^{(s+1)} - \tilde{\boldsymbol{\alpha}}^{(s+1)})^\top + 2\nu \text{diag}\left(1/\tilde{\lambda}_1^{(s)}, 1/\tilde{\lambda}_2^{(s)}\right)\right),$$

$$\tilde{\boldsymbol{\gamma}}^{(s+1)} \sim \text{N}_2\left(\tilde{\boldsymbol{\alpha}}^{(s+1)}, \tilde{\boldsymbol{\Gamma}}^{(s+1)}/K\right),$$

with $\tilde{\boldsymbol{\alpha}}^{(s+1)} = \frac{1}{K} \sum_{k=1}^K \tilde{\boldsymbol{\alpha}}_k^{(s+1)}$.

Given $\tilde{\boldsymbol{\Gamma}}^{(s+1)}$, simulate $\tilde{\lambda}_\ell, \ell = 1, 2$ via

$$\tilde{\lambda}_\ell^{(s+1)} \sim \text{Inverse Gamma}\left(1 + \nu/2, \frac{1}{\Lambda_\ell} + \nu(\tilde{\boldsymbol{\Gamma}}^{(s+1)})_{\ell\ell}^{-1}\right).$$

APPENDIX B: PHOTOMETRY DATA FOR WDS IN FIVE STAR CLUSTERS

Here are the photometry data for the WDs in these five star clusters in Section 4.

This paper has been typeset from a \LaTeX file prepared by the author.

Table B1. Photometry for the WDs in the Hyades

Cluster	WD	$U \pm \sigma_U$	$B \pm \sigma_B$	$V \pm \sigma_V$
Hyades	HZ14	9.155 ± 0.032	10.195 ± 0.030	10.351 ± 0.029
	VR16	9.298 ± 0.114	10.274 ± 0.114	10.373 ± 0.113
	HZ7	9.969 ± 0.025	10.859 ± 0.022	10.903 ± 0.016
	VR7	10.129 ± 0.049	10.977 ± 0.041	11.004 ± 0.035
	HZ4	11.136 ± 0.054	11.811 ± 0.054	11.725 ± 0.054
	LB227	11.034 ± 0.015	11.752 ± 0.015	11.697 ± 0.014

References: [DeGennaro et al. \(2009\)](#); [Stein et al. \(2013\)](#)**Table B2.** Photometry for the WDs in M67.

Cluster	WD	$B \pm \sigma_B$	$V \pm \sigma_V$
M67	WD 1	23.854 ± 0.010	23.505 ± 0.018
	WD 2	22.293 ± 0.010	22.047 ± 0.010
	WD 3	22.119 ± 0.010	21.910 ± 0.010
	WD 4	21.721 ± 0.010	21.646 ± 0.010
	WD 5	19.656 ± 0.010	19.837 ± 0.010
	WD 6	22.074 ± 0.010	21.834 ± 0.010
	WD 7	21.843 ± 0.010	21.611 ± 0.010
	WD 8	21.469 ± 0.010	21.290 ± 0.010
	WD 9	21.286 ± 0.010	21.152 ± 0.010
	WD 10	23.603 ± 0.010	23.224 ± 0.014
	WD 11	22.206 ± 0.010	21.899 ± 0.010
	WD 12	21.454 ± 0.010	21.216 ± 0.010
	WD 13	20.530 ± 0.010	20.527 ± 0.010
	WD 14	23.194 ± 0.010	22.820 ± 0.010
	WD 15	22.587 ± 0.010	22.275 ± 0.010
	WD 16	24.227 ± 0.010	23.693 ± 0.019
	WD 17	22.359 ± 0.010	22.061 ± 0.010
	WD 18	22.855 ± 0.010	22.493 ± 0.010
	WD 19	23.552 ± 0.010	23.181 ± 0.012
	WD 20	21.243 ± 0.010	21.204 ± 0.010
	WD 21	18.579 ± 0.010	18.890 ± 0.010
	WD 22	24.530 ± 0.013	23.970 ± 0.026
	WD 23	24.576 ± 0.013	24.053 ± 0.028
	WD 24	21.563 ± 0.010	21.298 ± 0.010
	WD 25	23.977 ± 0.010	23.610 ± 0.018
	WD 26	24.147 ± 0.010	23.678 ± 0.019
	WD 27	22.757 ± 0.010	22.413 ± 0.010
	WD 28	24.048 ± 0.010	23.641 ± 0.017
	WD 29	23.845 ± 0.010	23.444 ± 0.017
	WD 30	24.156 ± 0.010	23.979 ± 0.022
	WD 31	22.298 ± 0.010	22.022 ± 0.010
	WD 32	24.234 ± 0.010	23.838 ± 0.020
	WD 33	21.803 ± 0.010	21.573 ± 0.010
	WD 34	22.517 ± 0.010	22.172 ± 0.010
	WD 35	23.849 ± 0.010	23.299 ± 0.019

References: [Bellini et al. \(2010a,b\)](#)

Table B3. Photometry for the WDs in NGC188, NGC2168 and NGC2477.

Cluster	WD	$U \pm \sigma_U$	$B \pm \sigma_B$	$V \pm \sigma_V$	$I \pm \sigma_I$
NGC188	WD 1	22.651 ± 0.054	22.496 ± 0.124
	WD 2	23.350 ± 0.119	23.538 ± 0.386
	WD 3	23.490 ± 0.060	23.413 ± 0.185
	WD 4	23.508 ± 0.105	23.416 ± 0.559
	WD 5	23.669 ± 0.045	23.176 ± 0.149
	WD 6	24.206 ± 0.131	23.756 ± 0.228
	WD 7	24.439 ± 0.074	24.078 ± 0.255
	WD 8	24.469 ± 0.054	23.720 ± 0.195
	WD 9	25.261 ± 0.120	24.422 ± 0.297
NGC2168	WD 1	19.858 ± 0.019	20.953 ± 0.020	20.989 ± 0.019	...
	WD 2	20.532 ± 0.028	21.63 ± 0.031	21.569 ± 0.032	...
	WD 3	20.506 ± 0.020	21.364 ± 0.022	21.216 ± 0.020	...
	WD 4	18.764 ± 0.017	19.937 ± 0.018	20.065 ± 0.017	...
	WD 5	18.568 ± 0.017	19.735 ± 0.017	19.863 ± 0.016	...
	WD 6	20.339 ± 0.025	21.348 ± 0.028	21.303 ± 0.026	...
	WD 7	20.826 ± 0.023	21.759 ± 0.028	21.701 ± 0.027	...
	WD 8	19.727 ± 0.024	20.746 ± 0.024	20.785 ± 0.022	...
	WD 9	18.720 ± 0.018	19.665 ± 0.017	19.657 ± 0.016	...
	WD 10	20.479 ± 0.026	21.488 ± 0.029	21.398 ± 0.026	...
	WD 11	20.280 ± 0.025	21.650 ± 0.031	21.631 ± 0.029	...
	WD 12	19.558 ± 0.019	20.645 ± 0.019	20.719 ± 0.019	...
	WD 13	20.243 ± 0.020	21.170 ± 0.022	21.175 ± 0.020	...
NGC2477	WD 1	23.108 ± 0.008	22.816 ± 0.018
	WD 2	23.689 ± 0.010	23.237 ± 0.025
	WD 3	23.566 ± 0.011	23.282 ± 0.024
	WD 4	23.972 ± 0.016	23.638 ± 0.034
	WD 5	23.957 ± 0.015	23.586 ± 0.031
	WD 6	23.963 ± 0.015	23.576 ± 0.030
	WD 7	23.904 ± 0.012	23.461 ± 0.031

References for NGC188: [von Hippel & Sarajedini \(1998\)](#); [Meibom et al. \(2009\)](#)References for NGC2168: [Sung & Bessell \(1999\)](#); [Williams et al. \(2004\)](#)References for NGC2477: [Jeffery et al. \(2011\)](#); [Stein et al. \(2013\)](#)